



Lawrence Berkeley Laboratory

UNIVERSITY OF CALIFORNIA, BERKELEY

EARTH SCIENCES DIVISION

Submitted to the Journal of Geophysical Research

INJECTION AND THERMAL BREAKTHROUGH IN FRACTURED
GEOHERMAL RESERVOIRS

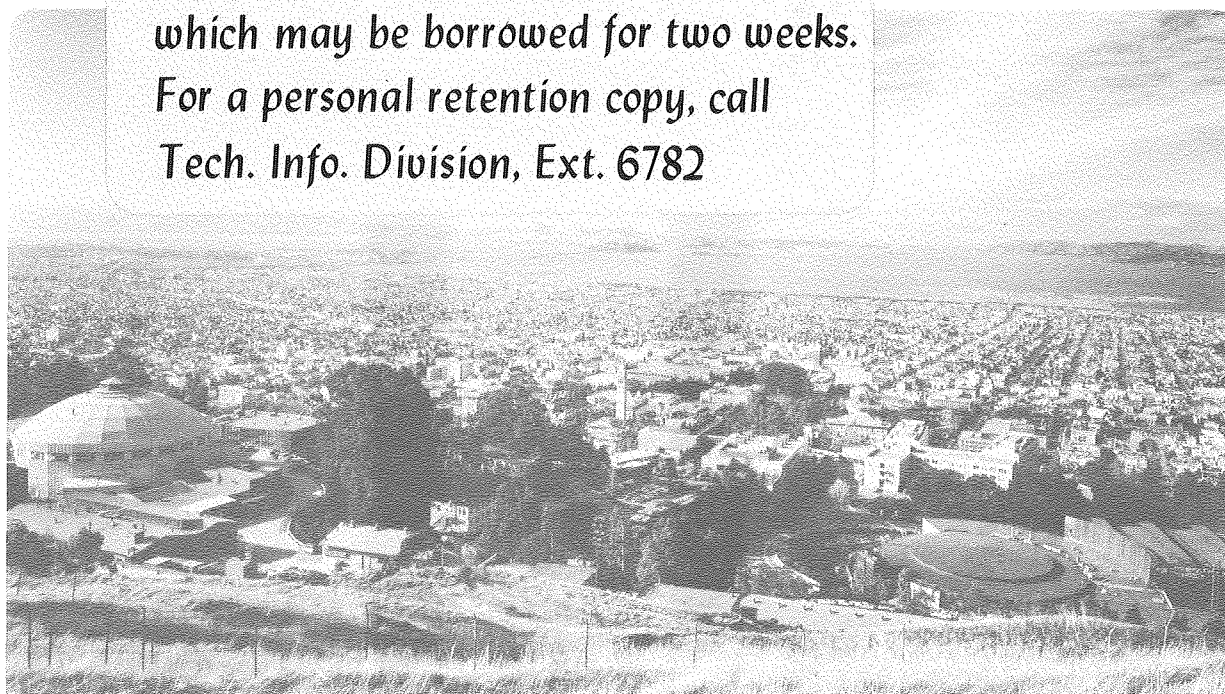
Gudmundur S. Bödvarsson and Chin Fu Tsang

May 1981

TWO-WEEK LOAN COPY

*This is a Library Circulating Copy
which may be borrowed for two weeks.
For a personal retention copy, call
Tech. Info. Division, Ext. 6782*

RECEIVED
LIBRARY
SEP 10 1981
JUN 30 1981
LIBRARY
DOCUMENTS



LBL-12698
c.2

DISCLAIMER

This document was prepared as an account of work sponsored by the United States Government. While this document is believed to contain correct information, neither the United States Government nor any agency thereof, nor the Regents of the University of California, nor any of their employees, makes any warranty, express or implied, or assumes any legal responsibility for the accuracy, completeness, or usefulness of any information, apparatus, product, or process disclosed, or represents that its use would not infringe privately owned rights. Reference herein to any specific commercial product, process, or service by its trade name, trademark, manufacturer, or otherwise, does not necessarily constitute or imply its endorsement, recommendation, or favoring by the United States Government or any agency thereof, or the Regents of the University of California. The views and opinions of authors expressed herein do not necessarily state or reflect those of the United States Government or any agency thereof or the Regents of the University of California.

INJECTION AND THERMAL BREAKTHROUGH
IN FRACTURED GEOTHERMAL RESERVOIRS

Gudmundur S. Bödvarsson and Chin Fu Tsang
Earth Sciences Division
Lawrence Berkeley Laboratory
University of California
Berkeley, CA 94720

May 1981

This work was supported by the Assistant Secretary for Resource Applications,
Office of Industrial & Utility Applications & Operations, Geothermal Energy
Division of the U.S. Department of Energy under Contract W-7405-ENG-48.

TABLE OF CONTENTS

List of Figures

Nomenclature

Abstract

1.0 Introduction

2.0 Basic Model

3.0 Analytical Study

3.1 Mathematical Model

3.2 Results of the Analytical Study

3.2.1 The Thermal Diffusion Process

3.2.2 Advancement of the Thermal Front Along the Fracture

3.2.2.1 Early-Time Behavior

3.2.2.2 Intermediate-Time Behavior

3.2.2.3 Late-Time Behavior

3.2.3 Advancement of the Thermal Front in the Rock Matrix

3.2.4 Temperature Distribution in the Fracture and in the Rock Matrix

4.0 Numerical Studies

4.1 Numerical Code

4.2 Comparison of Analytical and Numerical Results

4.3 The Importance of the Assumptions employed in the Analytical Approach

4.4 Considerations for Permeable Rock Matrix

4.4.1 Convection and Conduction

4.4.2 Convection-Dominated Systems

5.0 Practical Examples

5.1 Example 1

5.2 Example 2

6.0 Conclusions

Acknowledgements

References

Appendix A. Simultaneous Solution of Thermal Equations for Fracture and Rock

LIST OF FIGURES

1. Basic model of an injection well penetrating a reservoir with equally spaced horizontal fractures.
2. Schematic of analytical model.
3. Plots of thermal fronts at various dimensionless times, τ for $\theta < 0.01$; η is dimensionless vertical distance and ξ is dimensionless advancement along the fracture.
4. Plots of thermal fronts at various dimensionless times τ for $\theta > 100$.
5. Type curves for the movement of the thermal front in the fracture for various values of θ .
6. Advancement of the thermal front in the rock matrix for small values of θ .
7. Advancement of the thermal front in the rock matrix for large values of θ .
8. Temperature distribution in the fracture and rock matrix at various dimensionless times.
9. Diffuseness of the thermal front at intermediate times.
10. Diffuseness of the thermal front at late times.
11. The heat transfer mechanism in the system at late times for the reverse case -- hot-water injection into a colder reservoir.
12. Heat flux density along the fracture at late times. The parameter Q_d represents dimensionless energy loss from fracture to rock.
13. Schematic of the mesh used in the numerical calculations.
14. Comparison of the analytical and numerical results for $\theta = 0.01$.
15. The effects of numerical dispersion on the thermal front at various times.
16. Graphical integration showing an intermediate time thermal front isotherm as $T_D = 0.44$.
17. Comparison of analytical and numerical results (with relaxed assumptions) for advancement of the thermal front along the fracture.

LIST OF FIGURES - Continued

18. Temperature distribution in the rock matrix at various times; no horizontal conduction.
19. Thermal diffusion into the rock matrix at various times; horizontal conduction.
20. The late-time heat transfer mechanism for the rock-fracture system, when horizontal conduction is considered.
21. Effect of permeable rock matrix on the advancement of the thermal front along the fracture.
22. Schematic model of convection-dominated rock/fracture system.
23. Mesh used in the study of convection-dominated systems.
24. Pressure distribution along the dimensionless radial coordinate r_D for $\omega \leq 0.01$.
25. Pressure distribution along the dimensionless coordinate r_D for $\omega = 1$.
26. Pressure distribution along the dimensionless radial coordinate r_D for $\omega \geq 100$.
27. Dimensionless fluid flow along the fracture q_{HD} .
28. Cumulative flow from fracture to rock matrix.
29. Type curves developed for parameters considered in Example 1.
30. Geological model of the Cerro Prieto geothermal field (Example 2).

NOMENCLATURE

- A: Surface area (m^2)
- b: Fracture aperture (m)
- D: Thickness of rock matrix per fracture (equivalent to half the fracture spacing) (m)
- J_0 : Bessel function of the first kind, zero order
- J_1 : Bessel function of the first kind, first order
- k: Absolute permeability (m^2)
- n: Number of fractures
- p: Laplace parameter
- P: Pressure (pascals)
- P_D : Dimensionless pressure, $P_D = \frac{2\pi k_f b}{q\mu} \Delta P$
- ϕ : Porosity (-)
- q: The injection rate into each fracture (m^3/s)
- q_{FH} : Volumetric flow along the fracture (m^3/s)
- q_{HD} : Dimensionless mass flow along the fracture, $q_{HD} = \frac{q_{FH}}{q}$
- q_t : Total injection rate (m^3/s)
- Q_D : Dimensionless energy loss from rock matrix to fracture,
- $$Q_D = \frac{Q_H(2 + \theta)}{\rho_w c_w q (T_i - T_o)}$$
- Q_H : Energy loss from rock matrix to fracture.
- r: Radial coordinate (m)
- r_c : Radial distance from injection well to the location of uniform energy sweep
- r_D : Dimensionless radial distance, $r_D = \frac{r}{D}$

NOMENCLATURE - continued

R: Radial distance from injection well to the location of the thermal front

R_D : Dimensionless distance to constant pressure boundary, $R_D = \frac{r}{R_0}$

R_0 : Radial distance from injection well to the constant pressure boundary (m)

t: Time (seconds)

t_c : Time of uniform energy sweep (seconds)

t_D : Dimensionless time, $t_D = \frac{\lambda(t - t_c)}{\rho_r c_r r_c^2}$

T: Temperature (°C)

T_D : Dimensionless temperature, $T_D = \frac{T - T_0}{T_i - T_0}$

T_i : Injection temperature (°C)

T_0 : Initial temperature (°C)

T_{TF} : The isotherm defined as the "thermal front", generally $T_{TF} = (T_i + T_0)/2$

u: Temperature in fracture in Laplace domain

v: Temperature in rock matrix in Laplace domain

Y_0 : Bessel function of the second kind, zero order

Y_1 : Bessel function of the second kind, first order

z: Vertical coordinate (m)

ω : Dimensionless transmissivity, $\omega = \frac{D}{b} \frac{k_r}{k_f}$

η : Dimensionless vertical distance, $\eta = z/D$

θ : Dimensionless energy potential, $\theta = \frac{\rho_f c_f b}{\rho_r c_r D}$

NOMENCLATURE - continued

λ : Thermal conductivity of rock matrix (J/m·s·°C)

μ : Dynamic viscosity (kg/m·s)

ξ : Dimensionless distance, $\xi = \frac{\lambda \pi r^2 (2. + \theta)}{\rho_w c_w q \cdot D}$

ρc : Volumetric heat capacity (J/m³·°C)

τ : Dimensionless time, $\tau = \frac{\lambda t}{\rho_r c_r D^2}$

Subscripts:

f: Fracture

r: Rock matrix

w: Liquid water

ABSTRACT

In this study, the problem of cold water injection into a fractured geothermal reservoir is considered. During injection, the cold water will advance along the fractures, gradually extract heat from the adjacent rock matrix, and eventually arrive at the production wells. If the injected water has not fully heated up by then, detrimental effects on energy production from decreasing fluid enthalpies may result. This indicates the need to establish criteria for designing an injection/ production scheme for fractured geothermal reservoirs.

The model considered in this work consists of an injection well fully penetrating a fractured geothermal reservoir containing equally spaced horizontal fractures. A constant-temperature liquid water is injected into the fractures and with the rock matrix assumed to be impermeable, the effect of heat conduction on the advancement of the "cold" water along the fractures is observed. Key dimensionless parameters that describe the physical system are identified and type curves are generated. These are intended to be used in the design of injection/production systems, mainly for determining the appropriate locations and the flow rates of the injection wells. Also, temperature contour maps are given, and these can be used to estimate the amount of recoverable energy from the geothermal system, based on a given injection/production scheme.

Numerical studies are also made to investigate the importance of the assumptions in the analytical work and to extend the work to cases where the rock matrix is permeable. The results are intended to be used as a constraint on results calculated using the type curves.

1.0 INTRODUCTION

Reinjection of geothermal wastewater is gradually becoming a preferred means of waste disposal. At present, continuous reinjection is practiced at The Geysers, California^{1,2}; Ahuachapan, El Salvador^{3,4}; Mak Bau, Philippines⁵; and five Japanese geothermal fields (Otake, Onuma, Onikobe, Hatchobaru, and Kakkonda).^{5,6,7} Small-scale reinjection tests have been reported at a number of geothermal fields, e.g., Baca, New Mexico¹; East Mesa, California^{8,9}; Larderello, Italy¹⁰; Cerro Prieto, Mexico¹¹; Broadlands, New Zealand¹²; and Tangonan, Philippines.¹³ The increasing interest in reinjection undoubtedly results from growing environmental concerns regarding toxic minerals (e.g., boron, arsenic) present in geothermal wastewater.

Although reinjection currently is employed only as a means of wastewater disposal, it can greatly enhance the energy recovery from a geothermal field. The operators of The Geysers geothermal field are considering increasing the amount of injected water by using imported water, thereby attempting to take advantage of this important benefit of reinjection.¹⁰ A number of investigators have produced theoretical and numerical studies on the effect of reinjection on energy recovery from geothermal fields.¹⁴⁻¹⁸ Reinjection also aids in maintaining reservoir pressures. This has been illustrated at the Ahuachapan geothermal field, where direct correlation between the percentage of produced water injected and the reservoir pressure decline was found.¹⁹

The danger in employing reinjection is the possibility that the colder water will premature breakthrough from its zone around the injection well into the production region, thus drastically reducing the efficiency of the operation. The movement of the cold water (thermal front) in porous media type reservoirs is fairly well known from theoretical studies by various investigators.²⁰⁻²⁴ However, fluid movement in most geothermal reservoirs (except those in the

Imperial Valley) is controlled by fractures, a more complicated situation. It is generally believed that the cold water will advance very rapidly through the fractures and prematurely breakthrough at the production wells.

The objective of this paper is to investigate the advancement of the thermal front during injection into a fractured reservoir system. A reservoir system consisting of equally spaced horizontal fractures intersecting an injection well is considered. Analytical and numerical studies are carried out, addressing the important question of how fractures affect the movement of the thermal front during injection. Fundamental studies related to this problem have been reported by various researchers.^{14,25-28}

The experience gained from the large-scale reinjection experiments indicates that the advancement of the thermal front depends to a great extent on the geologic conditions that prevail at each geothermal site. Horne⁵ reports thermal interference in four of the five Japanese geothermal fields where reinjection is practiced (Onuma, Onikobe, Hatchobaru, and Kakkonda). However, at the Otake geothermal field, where reinjection has been employed since 1972,⁴ no thermal effects from reinjection have been observed. At Ahuachapan, premature thermal breakthrough has not occurred, although the water was injected at high flow rates for five years through an injection well located only 150 meters away from a good producer.¹⁹ These examples illustrate the basic need to study the advancement of the thermal front through fractured media so that criteria can be established for determining injection-well locations and flow rates based on some general geologic conditions. In the present study, such a criterion is developed for geothermal systems with horizontal fractures or layered reservoirs.

2.0 BASIC MODEL

The physical model considered is shown in Figure 1. The model consists of an injection well fully penetrating a reservoir with with a number, n , equally spaced horizontal fractures. The fractures are all identical with a constant aperture b and extend to infinity. The injection rate, q_t , is assumed to be constant and the same fluid mass, q , enters each fracture ($q_t = n \cdot q$). Gravity effects are neglected and, therefore, due to symmetry, only the basic section shown in Figure 1 needs to be considered.

In this study, the problem is approached using both analytical and numerical techniques, and this paper is subdivided accordingly. In the analytical work, the rock matrix associated with the fracture is assumed to be impermeable and therefore only the effects of thermal conduction are present. In the numerical study, most of the assumptions assumed in the analytical work are relaxed and cases where the rock matrix is permeable are considered.

3.0 ANALYTICAL STUDY

3.1 Mathematical Model

Figure 2 shows a schematic picture of the basic model considered in the analytical study. Besides the general assumptions discussed above, the following additional assumptions are made:

- 1) The flow in the fracture is steady and purely radial, with the well located at $r = 0$. The fracture of aperture b is at an elevation of $z = 0$ with the rock matrix extending vertically to $z = \pm D$.
- 2) Initially, the temperature is T_0 everywhere in the system, but at $t = 0$, the temperature of the injected water is fixed at T_i .
- 3) The fracture may contain some solids ($\phi_f < 1$) and an instantaneous thermal equilibrium between the fluid and the solids is assumed. Furthermore, in

the fracture, horizontal conduction is neglected and a uniform temperature in the vertical direction is assumed (infinite vertical thermal conductivity).

- 4) The rock matrix above and below the fracture is impermeable. Horizontal conduction is neglected and the vertical thermal conductivity is finite. No heat flow boundaries are assumed at $z = \pm D$.
- 5) The energy resistance at the contact between the fracture and the rock matrix is assumed to be negligible (infinite heat transfer coefficient) and therefore the fracture temperature is equal to the rock matrix temperature at the contact points ($z = \pm 0$).
- 6) No non-linearities are allowed, i.e., the density and heat capacity of the fracture fluids and solids, as well as the density, heat capacity, and thermal conductivity of the rock matrix are assumed to be constant.

The differential equation governing the fluid temperature in the fracture can be derived by performing energy balance in a control volume in the fracture. The derivation is similar to those reported by Lauwerier,²⁰ Bödvarsson,²⁶ and Gringarten et al.²⁷ The fracture equation is:

$$\left. \frac{1}{2\pi r} \frac{\rho_w c_w q}{b} \frac{\partial T_f}{\partial r} + \rho_f c_f \frac{\partial T_f}{\partial t} - \frac{2\lambda}{b} \frac{\partial T_r}{\partial z} \right|_{z=0} = 0 \quad [1]$$

where T_f is the temperature of the fluid in the fracture and T_r is the temperature in the rock matrix. Other parameters are defined in the nomenclature. The temperature in the rock matrix is governed by the one-dimensional heat conduction equation:

$$\frac{\partial^2 T_r}{\partial z^2} = \frac{\rho_r c_r}{\lambda} \frac{\partial T_r}{\partial t} \quad [2]$$

The initial and boundary conditions can be expressed as:

$$T_f(r,0) = T_r(r,z,0) = T_o \quad , \quad [3]$$

$$T_f(0,t) = \begin{cases} T_o & t < 0 \\ T_i & t \geq 0 \end{cases} \quad , \quad [4]$$

$$T_f(r,t) = T_r(r,0,t) \quad , \quad [5]$$

$$\left. \frac{\partial T_r}{\partial z} \right|_{z=D} = 0 \quad . \quad [6]$$

The dimensionless parameters ξ , τ , η , θ and T_D are defined as:

$$\xi = \frac{\lambda \pi r^2 (2 + \theta)}{\rho_w c_w q D} \quad , \quad [7]$$

$$\tau = \frac{\lambda t}{\rho_r c_r D^2} \quad , \quad [8]$$

$$\eta = \frac{z}{D} \quad , \quad [9]$$

$$\theta = \frac{\rho_f c_f b}{\rho_r c_r D} \quad , \quad [10]$$

$$T_D = \frac{T - T_o}{T_i - T_o} \quad . \quad [11]$$

Substituting equations (7)-(11) into Equations (1) and (2) yields:

$$\text{Fracture: } (2+\theta) \frac{\partial T_{Df}}{\partial \xi} + \theta \frac{\partial T_{Df}}{\partial \tau} - 2 \frac{\partial T_{Dr}}{\partial \eta} \Bigg|_{\eta=0} = 0 \quad [12]$$

$$\text{Rock: } \frac{\partial^2 T_{Dr}}{\partial \eta^2} = \frac{\partial T_{Dr}}{\partial \tau} \quad [13]$$

The initial conditions and the boundary conditions become:

$$T_{Df}(\xi, 0) = T_{Dr}(\xi, \eta, 0) = 0 \quad [14]$$

$$T_{Df}(0, \tau) = \begin{cases} 0 & \tau < 0 \\ 1 & \tau \geq 0 \end{cases} \quad [15]$$

$$T_{Df}(\xi, \tau) = T_{Dr}(\xi, 0, \tau) \quad [16]$$

$$\frac{\partial T_{Dr}}{\partial \eta} \Bigg|_{\eta=1} = 0 \quad [17]$$

Equations (12) and (13) along with the constraints given by Equations (14)-(17) form a coherent, self-sufficient set of equations. The simultaneous solution of the equations using the Laplace transformation is derived in Appendix A. In the Laplace domain the solutions for the fracture and the rock temperatures are:

$$\text{Fracture: } u = \frac{1}{p} \exp - [\theta p + 2\sqrt{p} \tanh \sqrt{p}] \xi \quad . \quad [18]$$

$$\text{Rock: } v = \frac{1}{p} \exp - [\theta p + 2\sqrt{p} \tanh \sqrt{p}] \xi \quad . \quad [19]$$

$$\{ \cosh \sqrt{p} \eta - \sinh \sqrt{p} \eta \tanh \sqrt{p} \}$$

where p is the Laplace parameter. Unfortunately, Equations (18) and (19) are difficult to invert analytically from the Laplace domain, so that a numerical inverter was used. The inverter was developed by Stehfest²⁹ and for this problem it gave results accurate within 0.7%.

3.2 Results of the Analytical Study

3.2.1 The Thermal Diffusion Process

In the following discussion, the concept of a "thermal front" will frequently appear. Although conventionally "front" refers to a sharp disruption moving through matter, here the definition of the term "thermal front" will be based on the following expression:

$$R^2 = \frac{2}{T_i - T_o} \int_0^{\infty} (T_f(r) - T_o) r dr \quad . \quad [20]$$

In Equation (20), R denotes the radial distance from the injection well to the location of the thermal front. The definition given by equation (20) is derived on the basis of energy balance considerations, so that if diffusion is neglected, the location of the resulting sharp front would at any time be given by Equation (20). In the analytical work, the thermal front is basically

symmetrical and therefore its location coincides with the location of the isotherm representing the average of the temperature of the injected water and the initial reservoir temperature ($T_{TF} = [T_i + T_o]/2$).

Figures 3 and 4 show the thermal diffusion from the fracture to the rock matrix for $\theta < 10^{-2}$ and $\theta > 10$ respectively. The dimensionless parameter, θ , represents the ratio of the energy potential of the fracture to that of the rock. Low values of θ indicate negligible energy content in the fracture, while large values correspond to negligible energy content in the rock. For the problem at hand, θ will most likely be less than 10^{-2} for all practical purposes.

In Figures 3 and 4, each plotted line indicates the location of the thermal front at the specified dimensionless time. The figures show that during cold water injection into the fractured rock, the thermal front will advance very rapidly along the fracture at early times, as only a small amount of heat is obtained from the rock. Later on, however, as the available surface area for heat transfer from the rock to the fracture increases, the rate of advancement of the thermal front along the fracture decreases, and the cold front starts to penetrate the rock matrix. Eventually, the thermal front in the rock matrix catches up with the thermal front in the fracture at a time corresponding to $\tau \approx 1.0$, and after that a uniform energy sweeping mechanism will prevail. This particular diffusion process emerged from numerical studies performed earlier,²⁸ and these led to the present analytical work.

It is for academic reasons interesting to compare Figures 3 and 4. The primary difference is that the dimensionless advancement (ξ) of the thermal front along the fracture at any given dimensionless time (τ) is always less in the case of large θ (Figure 4). For large θ , the rock matrix does not affect

the movement of the thermal front along the fracture, so that the location of the thermal front along the fracture is at any given time governed by the following expression:

$$\frac{t}{r^2} = \frac{\pi b}{q} \frac{\rho_f c_f}{\rho_w c_w} \quad [21]$$

Equation (21), derived by Bödvarsson,²¹ applies to a single-layer radial system with insulated upper (caprock) and lower (basement) boundaries. This expression will be discussed further in later sections.

3.2.2 Advancement of the Thermal Front Along the Fracture

The rate of cold water advancement along the fracture is of course one of the major concerns in the present problem. In Figure 5, type curves representing the movement of the thermal front in the fracture ($\eta = 0$) are given for various values of θ . The characteristics of the curves are such that subdividing the discussion into three subsections -- early, intermediate, and late-time behavior -- is warranted.

3.2.2.1 Early Time Behavior

At early times, for a given value of θ , the relationship between the dimensionless distance ξ and the dimensionless time τ is:

$$\tau = \frac{\theta}{2 + \theta} \xi \quad [22]$$

Substitution of the physical quantities for the dimensionless variables (Equations (8)-(11)) yields equation (21). This indicates that at early times, the cold-water front (thermal front) advances along the fracture as if no rock matrix is present.

3.2.2.2 Intermediate-Time Behavior

At intermediate times, the rock will start to conduct heat to the fracture and consequently slow down the advancement of the cold-water front along the fracture. This is evident in Figure 5 by the convergence of each θ curve to the mother curve ($\theta = 0$).

At intermediate times the relationship between the dimensionless distance ξ and the dimensionless time τ can be expressed as:

$$\tau = \frac{4.396}{(2 + \theta)^2} \xi^2 \quad [23]$$

Substitution of Equations (7)-(11) into Equation (23) yields:

$$\tau = 4.396 \frac{\lambda \rho_r c_r}{(\rho_w c_w)^2} \left(\frac{\pi r^2}{q} \right)^2 \quad [24]$$

Equation (23) corresponds to the Lauwerier equation (20) as expressed by B dvarsson and Tsang.³⁰ The problem solved by Lauwerier is identical to the present problem, except that Lauwerier assumed an infinite outer rock boundary condition, which is a special case of our solution ($D \rightarrow \infty$). Equation (24) shows that the time, τ , is proportional to the radial distance to the fourth power. This indicates the power of the heat conduction and how it effectively retards the advancement of the thermal front along the fracture.

The transition between the early-time behavior and intermediate-time behavior occurs at dimensionless time and dimensionless distance given respectively by:

$$\tau = \frac{\theta^2}{4.396} \quad [25]$$

$$\xi = \frac{\theta(2 + \theta)}{4.396} \quad [26]$$

Equations (25) and (26) seem quite reasonable, since a large fracture aperture and consequently a large θ , limits and retards the effects of conduction.

In the case of fractured reservoirs, Equations (25) and (26) may not have much practical value, because the transition occurs at such a short time. However, when injection into layered reservoirs is considered, these equations may be useful. Rewriting Equations (25) and (26) in terms of real variables (Equations (7)-(11)) yields:

$$t = \frac{b^2}{4.396} \frac{(\rho_f c_f)^2}{\lambda \rho_r c_r} \quad [27]$$

$$r = \sqrt{\frac{q}{4.396 \cdot \pi \cdot b} \frac{\rho_w c_w \rho_f c_f}{\rho_r c_r \lambda}} \quad [28]$$

3.2.2.3 Late-Time Behavior

As evident in Figure 5, at large dimensionless times the θ dependence no longer exists and the following simple relation between the dimensionless time τ and the dimensionless distance ξ results:

$$\tau = \xi \quad [29]$$

Substituting real variables for the dimensionless ones in Equation (29) yields:

$$\frac{t}{r^2} = \frac{\pi(2\rho_r c_r D + \rho_f c_f b)}{\rho_w c_w q} \quad [30]$$

As is to be expected, Equation (30) is equivalent to Equation (21), but with combined fracture and rock matrix thermal parameters. Equation (30) can be further simplified in cases of very large or very small θ as follows:

$$\frac{t}{r^2} = \begin{cases} \frac{2\pi\rho_r c_r D}{\rho_w c_w q} & \theta \ll 2 \\ \frac{\rho_f c_f}{\rho_w c_w} \frac{\pi b}{q} & \theta \gg 2 \end{cases} \quad [31]$$

For fractured reservoirs, the former expression would apply, whereas the second expression ($\theta \gg 2$) may be useful in cases of stratified reservoirs with relatively small shale breaks (e.g., Cerro Prieto geothermal field in Mexico).

The transition from the intermediate-time solution to the long-time solution occurs when the conductive heat flow from the rock matrix to the fracture becomes affected by the no-heat-flow boundary condition at $\eta = 1$ (insulated at $z = D$). The transition occurs at the time and location given by the following equation:

$$\tau = \xi = \frac{(2 + \theta)^2}{4.396} \quad [32]$$

Substitution of Equations (7)-(11) into Equation (32) yields:

$$t_c = \frac{\rho_r c_r D^2}{4.396\lambda} \left(2 + \frac{\rho_f c_f b}{\rho_r c_r D} \right)^2 \quad [33]$$

$$r_c = \sqrt{\frac{\rho_w c_w q D}{4.396 \cdot \pi \cdot \lambda} \left(2 + \frac{\rho_f c_f b}{\rho_r c_r D} \right)}, \quad [34]$$

where t_c and r_c denote the time and radial distance from the injection well, when uniform energy sweep is achieved. Again, for very large or very small values of θ , Equations (33) and (34) can be simplified as follows:

$$t_c = \begin{cases} \frac{2\rho_r c_r D^2}{4.396\lambda} & \theta \ll 2.0 \\ \frac{b^2(\rho_f c_f)^2}{4.396\rho_r c_r \lambda} & \theta \gg 2.0 \end{cases} \quad [35]$$

$$r_c = \begin{cases} \frac{2\rho_w c_w q \cdot D}{4.396 \cdot \pi \cdot \lambda} & \theta \ll 2.0 \\ \frac{q \cdot b \cdot \rho_w c_w \rho_f c_f}{4.396 \cdot \pi \cdot \rho_r c_r \lambda} & \theta \gg 2.0 \end{cases} \quad [36]$$

Note that for a small θ , the time of uniform energy sweep depends only on the thermal properties of the rock matrix and the distance to the insulated boundary (D), but not on the flow rate, the fracture aperture and width or thermal parameters.

3.2.3 Advancement of the Thermal Front in the Rock Matrix

Figures 6 and 7 show the advancement of the thermal front in the rock matrix for small and large values of θ , respectively. The graphs show that the lower the value of η ($\eta = z/D$), the earlier the curve converges to the $\eta = 0$

curve, which represents the thermal front along the fracture. This relationship is certainly reasonable since, the lower the value of η , the closer to the fracture the observation point is. The curves in Figures 6 and 7 also show that, at low values of ξ , the dimensionless parameters ξ and τ behave independently (τ does not change with changes in ξ). This behavior can be explained in terms of Figures 3 and 4. At early times during injection, the isotherms in the rock matrix close to the injection well (small ξ) are parallel to the fracture (pure vertical heat flow). The horizontal temperature gradient is practically negligible. Therefore, for a given η , the thermal front will arrive at the same dimensionless time regardless of the value of ξ .

3.2.4 Temperature Distribution in the Fracture and the Rock Matrix

The temperature distribution in the system at various dimensionless times is shown in Figure 8. In the plots, temperature contours 0.1 - 0.9 are shown in steps of 0.1. The temperature contours representing the temperature of the injected water ($T_D = 1.0$) and the temperature of the native reservoir water ($T_D = 0.0$) are not shown, due to difficulties in tracing them with the numerical inverter. Although the basic phenomenon explaining the behavior shown in Figure 8 has already been discussed (with reference to Figures 3 and 4), the graphs in Figure 8 can be quite useful in determining thermal contamination from injection. Furthermore, the data plotted in Figure 8 may aid in estimating the recoverable energy from a geothermal system, given the exploitation scheme (well spacing, flow rates, etc.).

The temperature distribution along the fracture is shown in Figures 9 and 10 for intermediate and late times, respectively. At early times-- that is, at times before the influence of the rock matrix is felt--the thermal front in the fracture is sharp, since horizontal conduction in the fracture is

neglected. The thermal front, however, becomes diffuse as the energy flow between the fracture and the rock matrix begins. Figure 9 shows how diffuse the thermal front becomes during intermediate times (times after the rock matrix starts to contribute significant energy, but before the no-heat-flow boundary condition is felt at $\eta = 1$). The curve is characterized by a rather sharp front, but a very diffuse tail.

The temperature distribution in the fracture and in the rock matrix (i.e., for all values of η) at late times is shown in Figure 10. For hot-water injection into a colder reservoir, the reverse case, the late-time behavior is illustrated in Figure 11. The figure shows that a hot zone corresponding to the temperature of the injected water has been developed, with a transition zone further away from the injection well and a cold water zone still further away. The heat is transported by convection along the fracture until the transition zone is reached. In the transition zone, the heat is conducted vertically into the rock matrix, with a heat flux density as shown in Figure 12. The parameter Q_d represents a dimensionless energy loss from the fracture to the rock matrix. Q_H is the energy flux calculated by means of the Fourier law of heat conduction:

$$Q_H = \lambda \cdot A \left. \frac{\partial T}{\partial z} \right|_{z=0} \quad [37]$$

As Figure 12 shows, the maximum energy loss occurs at $\xi/\tau \approx 1$, that is, at the radial distance from the well corresponding to the location of the thermal front (see Equation (29)). Since θ is less than 0.01, practically all of the injected energy will be conducted to the rock matrix (the energy potential of the fracture is negligible to that of the rock matrix), and consequently the area under the curve in Figure 12 will equal unity.

As Figure 11 illustrates, in the analytical solution developed in this study, horizontal conduction is neglected. This assumption causes the concentrated area of heat transfer shown in Figure 12 and the resulting sharp front (Figure 10). The importance of this assumption will be discussed in a later section.

4.0 NUMERICAL STUDIES

In addition to the analytical work discussed above, parallel numerical studies were carried out. The objective of the numerical studies is twofold:

- 1) To study the importance of the assumptions made in the analytical work.
- 2) To extend the analytical work to cases where the rock matrix is permeable.

In the following sections, the computer code used in the study will be described and the results discussed.

4.1 Numerical Code

In the present study the numerical code PT (Pressure and Temperature) is used. The code, recently developed at Lawrence Berkeley Laboratory (LBL), simultaneously solves both the mass and the energy transport equations for a single-phase fluid flow in a fully-saturated medium. It employs the Integrated Finite Difference Method in discretizing the medium and formulating the governing equations.^{31,32} The set of nonlinear equations arising at each time step is solved by means of an iterative scheme and an efficient sparse solver.³³

The numerical code has been extensively tested against analytical solutions for mass and heat flow problems.³⁴ It is based upon the numerical model CCC,²³ which is well validated from field data. Further details of the numerical code PT are given by Bödvarsson et al.³⁵

4.2 Comparison of Analytical and Numerical Results

As a first step, the very problem considered in the analytical work was solved using the numerical code and applying the same assumptions as in the analytical work (see Section 3.1). Figure 13 shows a schematic view of the mesh used; because of symmetry, only half of the basic section shown in Figure 2 was modeled. The fracture elements (the bottom layer) are connected to two constant-pressure, constant-temperature boundary elements (large nodes) to insure constant mass flow and a constant injection temperature T_i .

The vertical lines dividing the rock mass into elements are dotted to illustrate that there are no horizontal connections between the rock elements and subsequently no horizontal conduction in the rock matrix. The fracture elements are connected to enable a steady mass flow, but the thermal conductivity of the fracture elements was set to zero. The nodal points of the fracture elements were placed at the rock-fracture boundary to satisfy the boundary condition that the temperature of the rock at $z = 0$ ($\eta = 0$) is identical to the fracture temperature. Finally, a very high rock thermal conductivity was used, so that only small temperature gradients would develop in the rock matrix and therefore minimize the space discretization errors. The fracture aperture of 10^{-4} meters was arbitrarily selected and a fracture spacing ($2\pi D$) of 0.02 meters. Fixing all volumetric heat capacities as unity ($\rho_w c_w = \rho_f c_f = \rho_r c_r = 1$), a value of $\theta = 0.01$ resulted.

Figure 14 shows the comparison between the analytical and the numerical results for $\theta = 0.01$. The figure shows an excellent agreement between the analytical and the numerical results. However, although Equation (20) was always used to determine the location of the thermal front, the equivalent isotherm was not always T_{TF} , the average of the temperature of the injected water and the initial reservoir temperature (see section 3.2.1). In the case

of the early-time simulation ($\tau \leq 10^{-4}$), T_{TF} is the proper isotherm, as the thermal front becomes diffuse due to numerical dispersion, but remains symmetrical (see Figure 15). However, in the simulations representing intermediate ($10^{-4} < \tau < 1.0$) and late times ($\tau \geq 1.0$), heat transfer between the fracture and the rock matrix is present, and the associated numerical dispersion yields a non-symmetrical thermal front. In these cases, the proper isotherm representing the thermal front was selected by using graphical integration as illustrated in Figure 16. Using this approach, the thermal front for the intermediate time simulation was selected as $T_D = 0.44$, but for the late-time simulation as $T_D = 0.33$.

4.3 The Importance of the Assumptions Employed in the Analytical Approach

In order to understand the importance of the assumptions employed in the analytical work, a number of computer runs using the numerical code MEAT were made. In these simulations some of the more critical assumptions listed in Section 3.1 were relaxed. Thus, a transient mass flow is considered with variable fluid properties $\rho(P,T)$, $\mu(T)$ and horizontal conduction both in the fracture and the rock matrix is allowed. The results showed that the steady-state mass-flow assumption is indeed very reasonable and does not lead to significant errors in the thermal field. When considering only the location of the thermal front, the assumption of no horizontal conduction in the rock matrix is also reasonable. Figure 17 shows the comparison between the analytical results and the numerical results (with transient mass flow and horizontal conduction) for the advancement of the thermal front along the fracture.

However, at late times, horizontal conduction will become the dominant means of heat transfer, both in the rock and in the fracture. Figures 18

and 19 show the thermal diffusion into the rock matrix at various times for the cases of no horizontal conduction and with horizontal conduction, respectively. The parameters and the mesh used in the simulation are given in Table 1. The figures show that before the thermal front in the rock catches up with the thermal front in the fracture ($\tau < 1.0$), the effects of horizontal conduction are negligible. This is reasonable, since at early times the vertical temperature gradients are orders of magnitude larger than the horizontal gradients (see Figure 8). However, after uniform sweeping conditions prevail, the horizontal conduction dominates and eventually, when the fluid velocity in the fracture becomes very small (radial effects), the thermal front will advance purely through conduction. This mechanism is shown schematically in Figure 20.

The importance of horizontal conduction when uniform sweep conditions are reached clearly indicates that the present analytical solution cannot be used to calculate the temperature distribution at late times. An approximate solution can, however, be obtained using the finite radius solution by Van Everdingen and Hurst.³⁶ After adapting the solution to the present problem, it becomes:

$$T_D(r_D, t_D) = \frac{2}{\pi} \int_0^{\infty} \frac{[1 - \exp(-u^2 t_D)] [J_1(u)Y_0(ur_D) - (Y_1(u)J_0(ur_D))] du}{u^2 [J_1^2(u) + Y_1^2(u)]} \quad [38]$$

$$\text{where } T_D = \frac{T - T_i}{T_o - T_i}, \quad [39a]$$

$$t_D = \frac{\lambda(t - t_c)}{\rho_r c_r r_c^2}, \quad [39b]$$

$$r_D = \frac{r}{r_c} \quad [39c]$$

The symbol r_c denotes the radial distance from the injection well to the location where uniform sweep begins, and can be calculated using Equation (34); t is the time since injection began, and t_c is the time uniform sweep conditions start and can be calculated using Equation (33). The primary assumption made when the temperature distribution is calculated using Equation (38) is that a sharp front exists at $t = t_c$. At time $t = t_c$, the front is actually not very diffuse, as illustrated in Figure 10, and the assumption is probably reasonable, especially at late times ($t \gg t_c$). Equation (38) may be useful in estimating the temperature at the production well in cases of thermal breakthrough.

4.4 Considerations for Permeable Rock Matrix

In the analytical work, the assumption of an impermeable rock matrix was made. When the rock is permeable, heat transfer by convection between the fracture and the rock matrix will take place, in addition to the conductive heat transfer. The thermal front along the fracture (Figure 5) will therefore advance more slowly than the analytical solution predicts. In addressing this problem, the following approach was taken.

- 1) The non-isothermal mode of program PT was used to calculate the advancement of the thermal front in the fracture with time for several values of $k_D = k_f/k_r$, where k_f is the permeability of the fracture and k_r is the permeability of the rock matrix.
- 2) By assuming that conduction is negligible compared to the convective heat transfer between the fracture and the rock matrix, the location of uniform sweep conditions is calculated, based on steady-state flow patterns.

In the following sections, these considerations will be discussed.

4.4.1 Convection and Conduction

In these calculations, a finite but non-zero permeability was assigned to the rock elements and cold water injected into the fracture elements. Only the most general case was studied:

- 1) Transient mass flow
- 2) Horizontal and vertical convection in the rock matrix and horizontal conduction in the fracture.
- 3) Horizontal and vertical permeability in the rock matrix, but of equal magnitude (no anisotropy)
- 4) Nonconstant fluid parameters

$$\rho = f(P,T)$$

$$\mu = f(T)$$

The parameters used in the study are listed in Table 2 along with the grid spacings. In general, a uniform spacing is used in regions where temperature changes are expected, but logarithmic spacing in regions of the rock where isothermal flow is anticipated. The computer runs were made using only one set of geometric parameters, $\theta = 10^{-2}$, but a number of different values of dimensionless permeability k_D were used. The results for the advancement of the thermal front in the fracture are shown in Figure 21.

The results show that the rock permeability can have a large effect on the movement of the thermal front, and understandably, at any given time the higher the permeability of the rock matrix, the more the movement of the thermal front in the fracture will be retarded. The results in Figure 21 also indicate that if the permeability ratio k_D is greater than 10^4 the effect of the convective heat transfer is negligible. However, one must bear in mind

that these results are only valid for the set of parameters listed in Table 2, although they are expressed in a dimensionless form in Figure 21. For any arbitrary set of parameters independent calculations are required.

4.4.2 Convection Dominated Systems

The calculations presented in the last section show that convection due to a permeable rock matrix can considerably affect the thermal diffusion into the rock during injection. In this section, cases where the heat transfer between the fracture and the rock matrix are dominated by convection are considered. By neglecting conduction, one only needs to follow the fluid particles to find out where the heat is being transported.

In this study, the basic model shown in Figure 22 is used. As before, this model is valid for any number of equally spaced fractures. The following assumptions are employed.

- 1) The water is injected into the fracture at $r = 0$.
- 2) The mass flow is steady, and all fluid and rock parameters are constant.
- 3) In the fracture, only radial flow is considered; in the rock matrix both radial and vertical flow are considered.
- 4) A constant pressure boundary is located at $r = R_0$. Otherwise, the geometry of the problem is identical to problem discussed in the analytical work.
- 5) The fracture has a permeability k_f and the rock matrix has a permeability k_r in both r and z directions (no anisotropy).

Based on the model shown in Figure 22 and the above assumptions, mass balance on elements in the fracture and the rock matrix yield the following equations:

$$\text{Fracture: } \left. \frac{\partial^2 P_f}{\partial r^2} + \frac{1}{r} \frac{\partial P_f}{\partial r} + \frac{2k_r}{bk_f} \frac{\partial P_r}{\partial z} \right|_{z=0} = 0 \quad [40]$$

$$\text{Rock Matrix: } \frac{\partial^2 P_r}{\partial r^2} + \frac{1}{r} \frac{\partial P_r}{\partial r} + \frac{\partial^2 P_r}{\partial z^2} = 0 \quad [41]$$

The boundary conditions can be expressed mathematically as:

$$P_f(R_o) = 0 \quad [42A]$$

$$\lim_{r \rightarrow 0} r \left. \frac{\partial P_f}{\partial r} \right|_{r=0} = \frac{q\mu}{2\pi k_f b} \quad [42B]$$

$$P_f(r) = P_r(r, 0) \quad [42C]$$

$$\left. \frac{\partial P_r}{\partial r} \right|_{r=0} = 0 \quad [42D]$$

$$\left. \frac{\partial P_r}{\partial z} \right|_{z=0} = 0 \quad [42E]$$

$$P_r(R_o, z) = 0 \quad [42F]$$

Now introduce the following dimensionless parameters:

$$r_D = \frac{r}{D} \quad [43A]$$

$$\eta = \frac{z}{D} \quad [43B]$$

$$R_D = \frac{r}{R_o} \quad [43C]$$

$$\omega = \frac{D k_r}{b k_f} \quad [43D]$$

$$P_D = \frac{2\pi k_f b}{q\mu} P \quad [43E]$$

Substituting Equation (43) into Equations (40) and (41) yields:

$$\text{Fracture: } \left. \frac{\partial^2 P_{Df}}{\partial r_D^2} + \frac{1}{r_D} \frac{\partial P_{Df}}{\partial r_D} + 2\omega \frac{\partial P_{Dr}}{\partial \eta} \right|_{\eta = 0} = 0 \quad [44]$$

$$\text{Rock Matrix: } \frac{\partial^2 P_{Dr}}{\partial r_D^2} + \frac{1}{r_D} \frac{\partial P_{Dr}}{\partial r_D} + \frac{\partial^2 P_{Dr}}{\partial \eta^2} = 0 \quad [45]$$

The boundary conditions given by Equations (43) become:

$$P_{Df}(R_D = 1) = 0 \quad [46A]$$

$$\lim_{r_D \rightarrow 0} r_D \frac{\partial P_{Df}}{\partial r_D} = 1 \quad [46B]$$

$$P_{D_f}(r_D) = P_{D_r}(r_D, 0) \quad [46C]$$

$$\left. \frac{\partial P_{D_r}}{\partial r_D} \right|_{r_D = 0} = 0 \quad [46D]$$

$$\left. \frac{\partial P_{D_r}}{\partial \eta} \right|_{\eta = 1} = 0 \quad [46E]$$

$$P_{D_r}(R_D = 1, \eta) = 0 \quad [46F]$$

The above equations were solved numerically using the computer code MEAT in its isothermal mode. The mesh used is shown in Figure 23. The main characteristics of the mesh is that it logarithmically spaced both radially and vertically, and the nodal points are located at the log-mean center of the nodes. This type of grid setting has proven to be most accurate for diffusive-type problems. The grid was tested by running the Theis problem³⁷ with a constant pressure boundary (the solution is given in reference 38, Appendix L) and the results were within 1% of the analytical solution.

The pressure distribution along the dimensionless radial coordinate r_D is shown in Figures 24-26 for $\omega \leq .01$, $\omega = 1$, and $\omega > 100$, respectively. In all cases the distance to the constant pressure boundary R_0 is very large. This parameter has no significant effects on the results if it is specified large enough so as not to effect the fluid flow near the well.

The curves in Figures 24-26 show a number of interesting characteristics. First, in all cases the curves converge around $r_D = 1.0$. This indicates

that at radial distances from the well greater than that corresponding to $r_D = 1$ no vertical pressure gradient exists, and consequently, no flow between the fracture and the rock matrix takes place. Figures 24-26 also show that close to the well (r_D is small) there is no radial (horizontal) pressure gradient in the rock matrix. In explaining these characteristics, it is helpful to consider the fluid flow in the system. Figure 27 shows the dimensionless flow along the fracture with q_{HD} , defined as:

$$q_{HD} = \frac{q_{FH}(r)}{q} \quad [47]$$

where $q_{FH}(r)$ is the flow along the fracture, and q is the total flow. In this plot all of the curves also converge at $r_D \leq 1.0$ to a single curve that can be represented by the equation:

$$q_{HD}(1 + 2\omega) = 1 \quad [48]$$

expanding Equation (47) by using Darcy's law and rearranging yields:

$$q_{HD} = \frac{-\frac{k_f}{\mu} 2\pi r b \left(\frac{\partial P}{\partial r}\right)_f}{-\frac{k_f}{\mu} 2\pi r b \left(\frac{\partial P}{\partial r}\right)_f - \frac{k}{\mu} 2\pi r D \left(\frac{\partial P}{\partial r}\right)_r} = \frac{1}{1+2\omega} \quad [49]$$

It is obvious that Equation (49) is satisfied only when:

$$\left(\frac{\partial P}{\partial r}\right)_f = \left(\frac{\partial P}{\partial r}\right)_r \quad [50]$$

which is exactly the behavior shown in Figures 24-26. In other words, the flow from the fracture to the rock matrix takes place close to the well ($r_D < 1.0$); further away the flows in the fracture and the rock are governed only by the transmissibilities (k_{fb} and k_{rD}) of each.

The data plotted in Figure 27 also shows that very close to the well the flow in the fracture is constant and equal to the injection rate. Although the fluid flow from the fracture to the rock matrix per unit area is largest close to the well, the surface area there is small and consequently the total flow is small. The cumulative flow from the fracture to the rock matrix is plotted in Figure 28. Note that the horizontal axis is now defined as $r_D(1 + \omega)$. In Figure 28, there are two limiting curves representing high and low values of ω or equivalently high and low rock transmissibility. The figure shows that most of the flow between the fracture and the rock matrix takes place over the interval:

$$10^{-2} < r_D(1 + \omega) < 10 \quad [51]$$

The scaling of the dimensionless radial coordinate with the dimensionless parameter ω , is due to the fact that the higher the rock permeability, the closer to the well significant vertical flow will occur.

The implications for the cold-water injection problem are quite obvious. If the conductive heat transfer is negligible, all of the heat exchange from the fracture to the rock will take place within the dimensionless distance $r_D = 1$ from the well. In cases where the rock-matrix permeability is not negligible, this can be used as a constraint on the basic type curves shown in Figure 5. It should, however, be emphasized that this constraint can only be used in cases where $\omega > 10$, since ω represents the ratio of the convective heat flows in the rock and in the fracture. For example, if ω is 1.0, only 50% of the energy will enter the rock matrix.

5.0 PRACTICAL EXAMPLES

5.1 Example 1

In many geothermal fields in volcanic rocks the major fluid conduits are the contacts between subsequent lava layers.³⁹⁻⁴² These contacts may extend over a large area and behave hydrologically as horizontal fractures of large areal extent. As an example, consider a 1000-meter-thick geothermal reservoir consisting of six rather impermeable layers with the contact points between the layers being the principal fluid conduits. The number of high permeability contact zones is not precisely known, but a spinner survey indicates the presence of two to five major zones. An abandoned production well is located 250 m away from the closest producer and the field developer is interested in knowing, if it were used as an injection well, when the injected water would break through at the production well. The fluid and reservoir data needed for calculations is shown in Table 3. Using the parameters in Table 3 and the type curves in Figure 5, the curves in Figure 29 were developed. To account for the effect of the production well on the velocity field, the injection rate was doubled before the data shown in Figure 29 was calculated. Now using a well spacing of 250 m, the thermal front will reach the production well in 13 and 65 years for two and five fractures, respectively. Since the planned life of the project in question was 15 years, and since the approach to the problem was conservative (no rock permeability, etc.), the developer was reasonably certain that premature breakthrough would not occur.

5.2 Example 2

In the second example, consider the geological model of the Cerro Prieto field reported by Tsang et al.⁴¹ and shown in Figure 30. In this

case, the aquifers are considered to be the major fluid conduits and the shale breaks the low permeability layers. The injection well is assumed to fully penetrate both of the aquifers and to supply the same quantity of cold water to each. Neglecting gravity, or assuming strong anisotropy, fixing the injection rate as 20 kg/s, and using the same rock and fluid thermal properties as are shown in Table 3, the advancement of the thermal front in the aquifers with time can be calculated. In this case, $\theta = 4.0$. In order to calculate when all of the energy from the shale layers can be extracted, Equation (33) can be used to yield:

$$t = 400 \text{ years} . \quad [52]$$

The radial distance to the point of uniform sweep can be calculated using Equation (34) as:

$$r = 1635 \text{ m} . \quad [53]$$

If the geothermal project is planned for 30 years, the cold water front will only have advanced 240 m away from the injection well. Now let us consider the case of two horizontal fractures in the aquifers in Figure 30. In this case, $D = 50$ m, and if the fracture aperture is 10^{-4} m, a fracture permeability of $8.33 \times 10^{-10} \text{ m}^2$ can be calculated using the cubic law⁴²:

$$k_f = \frac{b^2}{12} . \quad [54]$$

The permeability of the Cerro Prieto aquifers has been reported as approximately $6.5 \times 10^{-14} \text{ m}^2$ (ref. 43), and therefore $\omega \approx 40$. Recognizing that our analysis in Section 4.4.2 can be used, providing $\omega > 10$, a critical

radius of 50 m is calculated. Since the fractures will not affect the thermal front 50 m away from the well, our earlier calculation of 240 m in thirty years is valid in spite of the presence of the fractures.

6.0 CONCLUSIONS

In this study, the thermal behavior during cold-water injection into fractured geothermal reservoirs is considered. The model used consists of an injection well fully penetrating a geothermal reservoir with horizontal fractures. The approach employed in the study is twofold; first, a rather simple mathematical model is developed and solved analytically; second, numerical calculations are carried out in order to investigate the importance of the assumptions employed in the analytical study and extend the applicability of the results.

The results from the analytical work are given in the form of type curves that can be used to design the locations of the injection wells with reference to the production wells, and the injection rate. The type curves can also be used to predict the time of thermal breakthrough in existing injection/production systems. A number of curves showing the thermal contamination in the impermeable rock matrix (or adjacent layers) may be useful in calculating the recoverable energy in a reservoir system for given well locations and rates.

In the numerical study, the importance of the more critical assumptions employed in the analytical work were studied. The assumption of steady-state mass flow was found to be very reasonable, whereas the assumption of no horizontal conduction in the rock matrix (adjacent layer) gave erroneous temperature distributions at very late times. A method of approximating the temperature distribution at late times is suggested.

Finally, extension of the analytical work to include permeable rocks is studied numerically. A mathematical model is developed and key dimensionless parameters identified. The primary assumption used in this part of the work is that the conductive heat transfer is negligible compared to the convective heat transfer (high Peclet number). This enables one to consider only the stream lines under steady-state conditions. The problem is solved numerically using the computer code PT in its isothermal mode. The results obtained indicate that at radial distances from the injection well larger than the thickness of the rock matrix, uniform energy sweep conditions will develop. In certain cases ($\omega > 10$) this result can be used as a constraint on estimates obtained with the developed type curves.

ACKNOWLEDGMENTS

The authors express their gratitude to Göran Hellström for his contributions to this work. The work was supported by the Assistant Secretary for Resource Applications, Office of Industrial & Utility Applications & Operations, Geothermal Energy Division of the U.S. Department of Energy under Contract W-7405-ENG-48.

References

1. Chasteen, A.J., Geothermal steam condensate reinjection: in Proceedings Second United Nations Symposium, Vol. 2, San Francisco, California, (May) 1975.
2. Kruger, P., and Otte, C., Geothermal energy: Stanford University Press, Stanford, California, 1973.
3. Einarsson, S.S., Vides, A.R., and Cuellar, G., Disposal of geothermal waste water by reinjection: in Proceedings Second United Nations Symposium, Vol. 2, San Francisco, California, (May) 1975.
4. Cuellar, G., Behavior of silica in geothermal waste waters: in Proceedings Second United Nations Symposium, Vol. 2, San Francisco, California, (May) 1975.
5. Horne, R., Geothermal reinjection experience in Japan: paper presented at the California Regional SPE meeting, Bakersfield, California, SPE-9925, (March 25-26) 1981.
6. Kubota, K., and Aosaki, K., Reinjection of geothermal hot water at the Otake geothermal field: in Proceedings Second United Nations Symposium, Vol. 2, San Francisco, California, (May) 1975.
7. Hayashi, M., Mimura, T., and Yamasaki, T., Geological setting of reinjection wells in the Otake and the Hatchobaru geothermal field, Japan: Transactions, Geothermal Resources Council, Vol. 2, p. 263-266, (July) 1978.
8. Mathias, K.E., The Mesa geothermal field--a preliminary evaluation of five geothermal wells: in Proceedings Second United Nations Symposium, Vol. 2, San Francisco, California, (May) 1975.
9. Benson, S.M., Goranson, C.B., McEdwards, D., and Schroeder, R.C., Well tests: in Geothermal resource and reservoir investigation of U.S. Bureau of Reclamation Leaseholds at East Mesa, Imperial Valley, California, LBL-7094, (October) 1978.
10. Pruess, K., private communication.
11. Vides, A., Recent studies of the Ahuachapan geothermal field: in Proceedings Second United Nations Symposium, Vol. 2, San Francisco, California, (May) 1975.
12. Brixley, P.F., and Grant, M.A., Reinjection testing at Broadlands: in Proceedings of the 4th Workshop on Geothermal Reservoir Engineering, Stanford University, 1979.
13. Studt, F.E., Geothermal fluid injection-experience in New Zealand and the Philippines: paper presented at the NATO CCMS Geothermal Conference, Paris, France, (July 15) 1980.
14. Kasameyer, P., and Schroeder, R., Thermal depletion of liquid-dominated geothermal reservoirs with fracture and pore permeability: UCRL-77323 preprint, (December) 1975.

References - Continued

15. Pritchett, J.W., Garg, S.K., and Riney, T.D., Numerical simulations of the effects of reinjection on performance of a geopressured geothermal reservoir: Transactions, Geothermal Resource Council, Vol. 1, 1977.
16. Lippmann, M.J., Tsang, C.F., and Witherspoon, P.A., Analysis of the response of geothermal reservoirs under injection and production procedures: presented at the 47th Regional Meeting of the SPE, Bakersfield, California, SPE-6537, 1977.
17. O'Sullivan, M.J., and Pruess, K., Analysis of injection testing of geothermal reservoirs: Geothermal Resources Council, Vol. 4., (September) 1980.
18. Schroeder, R.C., O'Sullivan, M.J., and Pruess, K., Reinjection studies of vapor-dominated systems: paper presented at the Italian-American Workshop, Berkeley, California, (October) 1980.
19. Witherspoon, P.A., private communication.
20. Lauwerier, H.A., The transport of heat in an oil layer caused by the injection of hot fluid: Appl. Sci. Res. Scat. A., 5, 145, 1955.
21. Bödvarsson, G., Thermal problems in the siting of reinjection wells: Geothermics, Vol. 1, No. 2, 1972.
22. Gringarten, A.C., and Sauty, J.P., A theoretical study of heat extraction from aquifers with uniform regional flow: Journal of Geophysical Research, Vol. 80, No. 5, p. 4956, 1975.
23. Lippmann, M.J., Bödvarsson, G.S., Witherspoon, P.A., and Rivera R., J., Preliminary simulation studies related to the Cerro Prieto field: Geothermics, Vol. 9, p. 197-207, 1980.
24. Tsang, C.F., Bödvarsson, G.S., Lippmann, M.J., and Rivera R., J., A study of alternate reinjection schemes for the Cerro Prieto geothermal field, Baja California, Mexico: Transactions of the Geothermal Resources Council, 1978.
25. Romm, E.S., On one case of heat transfer in fractured rock: All-Union Institute for Scientific Research and Geological Exploration for Petroleum, U.S.S.R., preprint.
26. Bödvarsson, G., On the temperature of water flowing through fractures: J. Geophys. Res., Vol. 74, No. 8, (April) 1969.
27. Gringarten, A.C., Witherspoon, P.A., and Onishi, Y., Theory of heat extraction from fractured hot dry rock: J. Geophys. Res., Vol. 80, No. 8, (March) 1975.
28. Bödvarsson, G.S., and Tsang, C.F., Injection into a fractured geothermal reservoir: Transactions, Vol. 4, Geothermal Resources Council, (September) 1980.

References - Continued

29. Stehfest, H., Numerical inversion of Laplace transforms: Communications of ACM, Vol. 13, p. 44-49, 1979.
30. Bödvarsson, G.S., and Tsang, C.F., Injection into fractured geothermal reservoirs: Annual Report of the Earth Science Division of Lawrence Berkeley Laboratory, 1980.
31. Edwards, A.L., TRUMP: A computer program for transient and steady state temperature distribution in multidimensional systems: Lawrence Livermore Laboratory, UCRL-14754, Rev. 3, 1972.
32. Narasimhan, T.N., and Witherspoon, P.A., An integrated finite differences method for analyzing fluid flow in porous media: Water Resources Res., Vol. 12, No. 1, p. 57-64, 1976.
33. Duff, I.S., MA28--A set of Fortran subroutines for sparse unsymmetric linear equations: Report AERE - R 8730, Harwell/Oxfordshire, Great Britian, 1977.
34. Bödvarsson, G.S., Numerical modeling of geothermal systems: Ph.D. thesis in preparation.
35. Bödvarsson, G.S., and Lippmann, M.J., Recent modifications of the computer code CCC: Annual Report of the Earth Sciences Division of Lawrence Berkeley Laboratory, 1979.
36. Van Everdingen, A.F., and Hurst, W., The application of Laplace transformation to flow problems in reservoirs: TRANS AIME, Vol. 186, 305, 1949.
37. Theis, C.V., The relationship between the lowering of piezometric surface and the rate and duration of discharge using groundwater storage: Transactions American Geophysical Union, Vol. 2, p. 519-524, 1935.
38. Witherspoon, P.A., Javandel, I., Neuman, S.P., and Freeze, R.A., Interpretation of aquifer gas storage conditions from water pumping tests: monograph published by the American Gas Association, 1967.
39. Fridleifsson, I.B., Lithology and structure of geothermal reservoir rocks in Iceland: Proceedings Second United Nations Symposium, San Francisco, California, (May) 1975.
40. Newcomb, R.C., Strand, J.R., and Frank, F.J., Geology and groundwater characteristics of the Hanford Reservation of the U.S. Atomic Energy Commission, Washington, Geological Survey professional paper 717, 1972.
41. O'Brien, M., Benson, S.M., and Goranson, C.B., Subsurface geology of three geothermal wells, Klamath Falls, Oregon, Lawrence Berkeley Laboratory, LBL-11240 1981.
42. Benson, S.M., Goranson, G.B., Noble, J., Schroeder, R., Corrigan, D., and Wollenberg, H., Evaluation of the Susanville, California geothermal resource: Lawrence Berkeley Laboratory, LBL-11187, 1981.

References - Continued

43. Tsang, C.F., Mangold, D.C., and Lippmann, M.J., Simulation of reinjection at Cerro Prieto using an idealized two-reservoir model: Proceedings of the Second Symposium on the Cerro Prieto geothermal field, Baja California, Mexico, (October 17-19) 1979.
44. Witherspoon, P.A., Wang, J.S.Y., Iwai, K., and Gale, J.R., Validity of Cubic law for fluid flow in a deformable rock fracture: Water Resources Research, Vol. 16, No. 6, p. 1016-1024, 1980.

APPENDIX A - Simultaneous Solution of Thermal Equations for Fracture and Rock

In dimensionless form, the equation governing the temperature in the fracture and the rock are:

$$\text{Fracture: } (2+\theta) \frac{\partial T_{Df}}{\partial \xi} + \theta \frac{\partial T_{Df}}{\partial \tau} - 2 \frac{\partial T_{Dr}}{\partial \eta} \Bigg|_{\eta=0} = 0 \quad (\text{A1})$$

$$\text{Rock: } \frac{\partial^2 T_{Dr}}{\partial \eta^2} = \frac{\partial T_{Dr}}{\partial \tau} \quad (\text{A2})$$

The initial and boundary conditions are:

$$T_{Df}(\xi, 0) = T_{Dr}(\xi, \eta, 0) = 0 \quad , \quad (\text{A3})$$

$$T_{Df}(0, \tau) = \begin{cases} 0 & \tau < 0 \\ 1 & \tau > 0 \end{cases} \quad , \quad (\text{A4})$$

$$T_{Df}(\xi, t) = T_{Dr}(\xi, 0, \tau) \quad , \quad (\text{A5})$$

$$\frac{\partial T_{Dr}}{\partial \eta} \Bigg|_{\eta=1} = 0 \quad . \quad (\text{A6})$$

After applying Laplace transformation with respect to τ , Equations (A1) and (A2) become:

$$(2+\theta) \frac{\partial u}{\partial \xi} + \theta pu - 2 \frac{\partial v}{\partial \eta} \Bigg|_{\eta=0} = 0 \quad , \quad (\text{A7})$$

$$\frac{\partial^2 v}{\partial \eta^2} - pv = 0 \quad , \quad (A8)$$

where u and v are the temperatures of the fracture and the rock matrix in the Laplace space, respectively. In the Laplace domain, the boundary conditions (Equations (A4)-(A7)) become:

$$u(0) = 1/p \quad (A9)$$

$$u(\xi) = v(\xi, 0) \quad (A10)$$

$$\left. \frac{\partial v}{\partial \eta} \right|_{\eta=1} = 0 \quad (A11)$$

The solution to Equation (A9) is:

$$v = A \cosh \sqrt{p} \eta + B \sinh \sqrt{p} \eta \quad , \quad (A12)$$

where A and B are constants. Applying boundary conditions given by Equations (A10) and (A11), A and B can be determined:

$$B = -A \tanh \sqrt{p} \quad , \quad (A13)$$

$$A = u \quad (A14)$$

Substituting Equations (A13) and (A14) into (A12) yields:

$$v = u(\cosh \sqrt{p} \eta - \sinh \sqrt{p} \eta \tanh \sqrt{p}) \quad (A15)$$

Now prepare to solve the equation for the temperature in the fracture (Equation (A8)):

$$\left. \frac{\partial v}{\partial \eta} \right|_{\eta=0} = -u\sqrt{p} \tanh \sqrt{p} \quad . \quad (A16)$$

Substitution of Equation (A16) into Equation (A8) yields:

$$(2+\theta) \frac{du}{d\xi} + \theta pu + 2u \sqrt{p} \tanh \sqrt{p} = 0 \quad (A17)$$

rewriting (A17):

$$\frac{du}{d\xi} + \frac{(\theta p + \sqrt{p} \tanh \sqrt{p}) \xi}{(2 + \theta)} = 0 \quad (A18)$$

The solution of Equation (A20) is:

$$U = C \exp - \frac{(\theta p + 2\sqrt{p} \tanh \sqrt{p}) \xi}{(2 + \theta)} \quad (A19)$$

Applying boundary conditions given by Equation (A9) enables determination of the constant C as $C = 1/p$ and Equation (A19) becomes:

$$u = \frac{1}{p} \exp - \frac{(\theta p + 2\sqrt{p} \tanh \sqrt{p}) \xi}{(2 + \theta)} \quad (A20)$$

Finally, having obtained a solution for the fracture temperature in the Laplace domain (u) one can write the complete solution for the rock temperature in the Laplace domain (v):

$$v = \frac{1}{p} \exp - \frac{(\theta p + 2\sqrt{p} \tanh \sqrt{p}) \xi}{(2 + \theta)} \quad (A21)$$

$$(\cosh \sqrt{p} \eta - \sinh \sqrt{p} \eta \tanh \sqrt{p})$$

TABLE 1: Parameters used in the study of the effects of horizontal conduction.

	Fracture (Fluid)	Rock Matrix
Thermal conductivity, $\lambda(\text{J}/\text{m}\cdot\text{s}\cdot^{\circ}\text{C})$	1.0	10.0
Density, $\rho(\text{kg}/\text{m}^3)$	1000.0	1000.0
Specific heat, $C(\text{J}/\text{kg}\cdot^{\circ}\text{C})$	1000.0	1000.0
Porosity, $\phi (-)$	1.0	.001

Fracture aperture b: 10^{-4} m

Fracture spacing 2D: 0.02 m

Flow rate Q: 1×10^{-2} m³/s

Mesh:

a) Radial spacing: 10 x 0.1 m, 20 x 1 m, 2, 3, 7, 8, 10,
15, 15, 20, 60, 90, 150, 250, 350 m

b) Vertical spacing: 5×10^{-5} , 1×10^{-5} , 3×10^{-5} , 1×10^{-4}
 3×10^{-4} , 1×10^{-3} , 3×10^{-3} , 5.556×10^{-3} m

TABLE 2: Parameters and grid spacing used in the non-isothermal permeable rock study.

	Fracture (Fluid)	Rock
Thermal conductivity, $\lambda(\text{J/m}\cdot\text{s}\cdot^\circ\text{C})$	1.0	2.0
Density, $\rho(\text{kg/m}^3)$	1000.0	2650.0
Specific Heat, $(\text{J/kg}\cdot^\circ\text{C})$	4200.0	1000.0
Porosity, $\phi (-)$	1.0	.01
Permeability $k(\text{m}^2)$	1×10^{-9}	1×10^{-9} - 1×10^{-16}
Compressibility $C(\text{Pa}^{-1})$	5×10^{-10}	5×10^{-10}

Fracture aperture b: 10^{-4} m

Fracture spacing 2D: 0.02 m

Flow rate Q: 1×10^{-2}

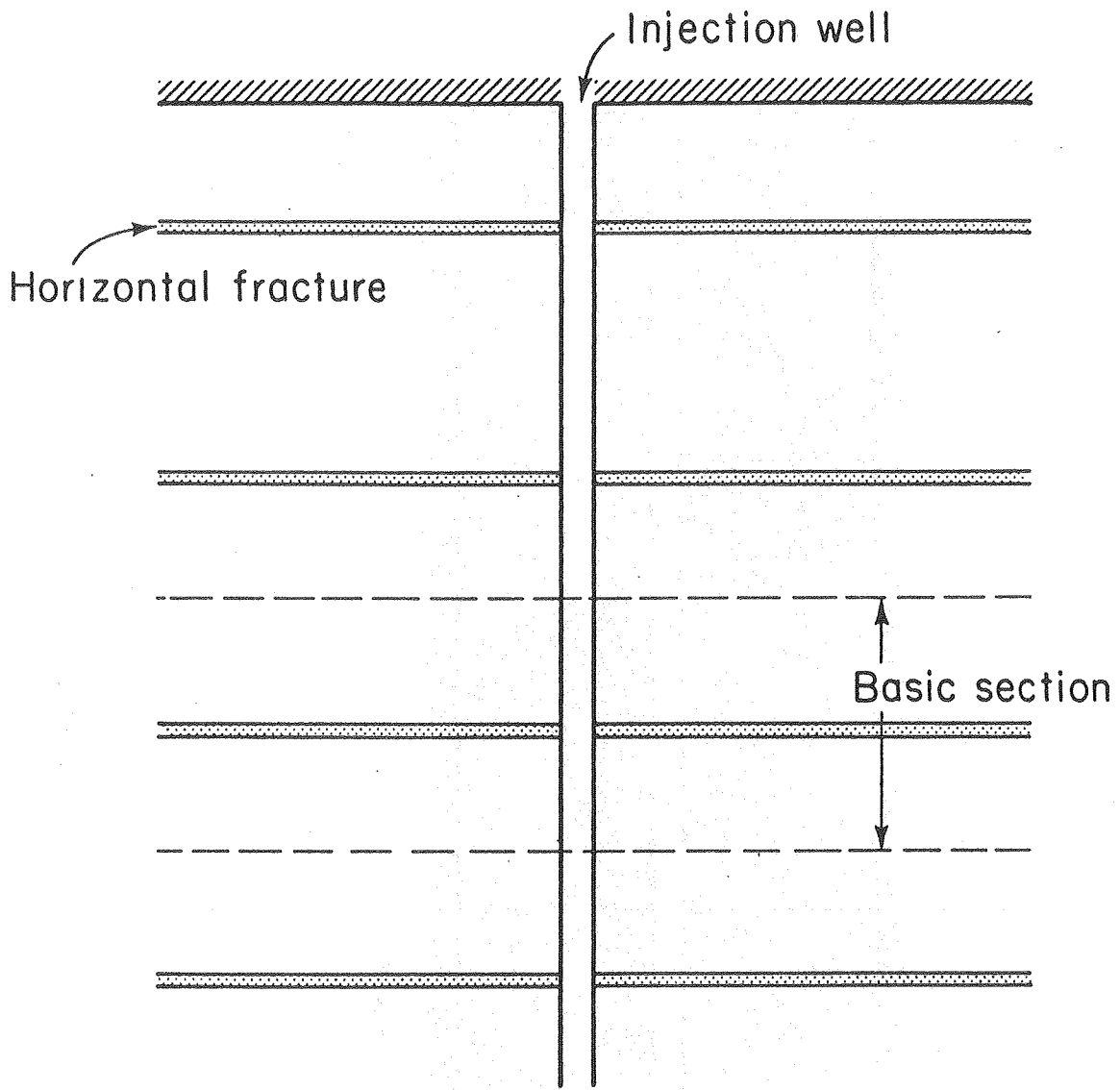
Mesh:

a) Radial spacing: 5×0.02 , 17×0.5 , .3, 0.5, 0.5, 0.7, 0.8, 1.0, 1.0, 1.5, 1.5, 2, 6, 15, 25, 35, 60, 90, 150, 250, 350 m, etc.

b) Vertical spacing: 5×10^{-5} , 1×10^{-5} , 3×10^{-5} , 1×10^{-4} , 3×10^{-4} , 1×10^{-3} , 3×10^{-3} , 5.56×10^{-3} m

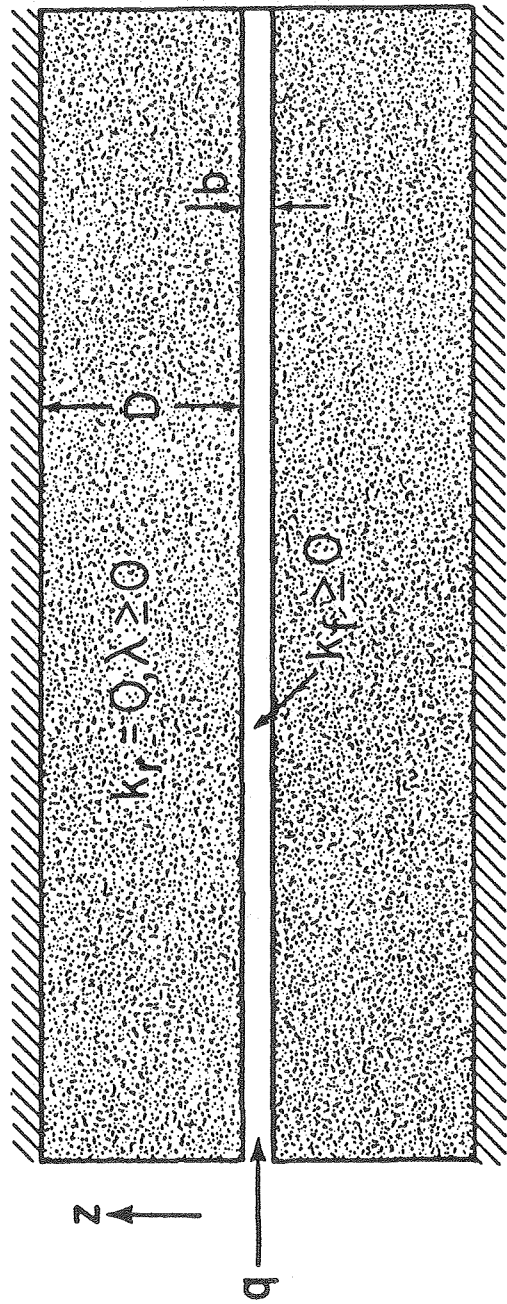
TABLE 3: Parameters used in Example 1.

Flowrate q , (kg/s):	10.0
Thermal conductivity λ (J/m·s·°C):	2.0
Fluid density ρ_w (kg/m ³):	1000
Fluid specific heat, c_w (J/kg·°C):	4000
Rock density ρ_r :	2500
Rock specific heat c_r (J/kg·°C):	1000
Fracture porosity, ϕ (-):	1.0
Fracture aperture, b (m):	1×10^{-4}



XBL 805-7081

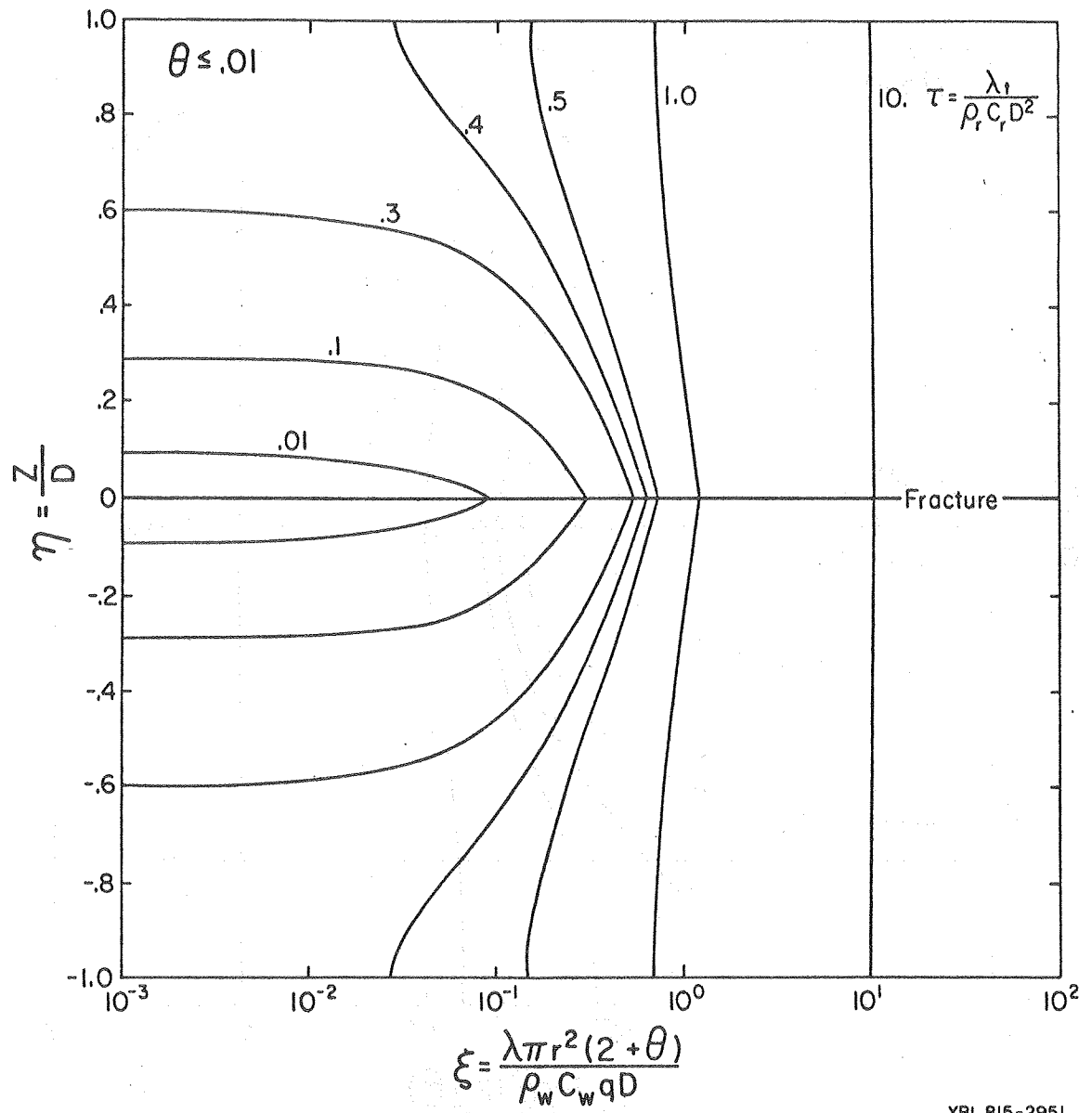
Figure 1



r

XBL 815-2968A

Figure 2



XBL 815-2951

Figure 3

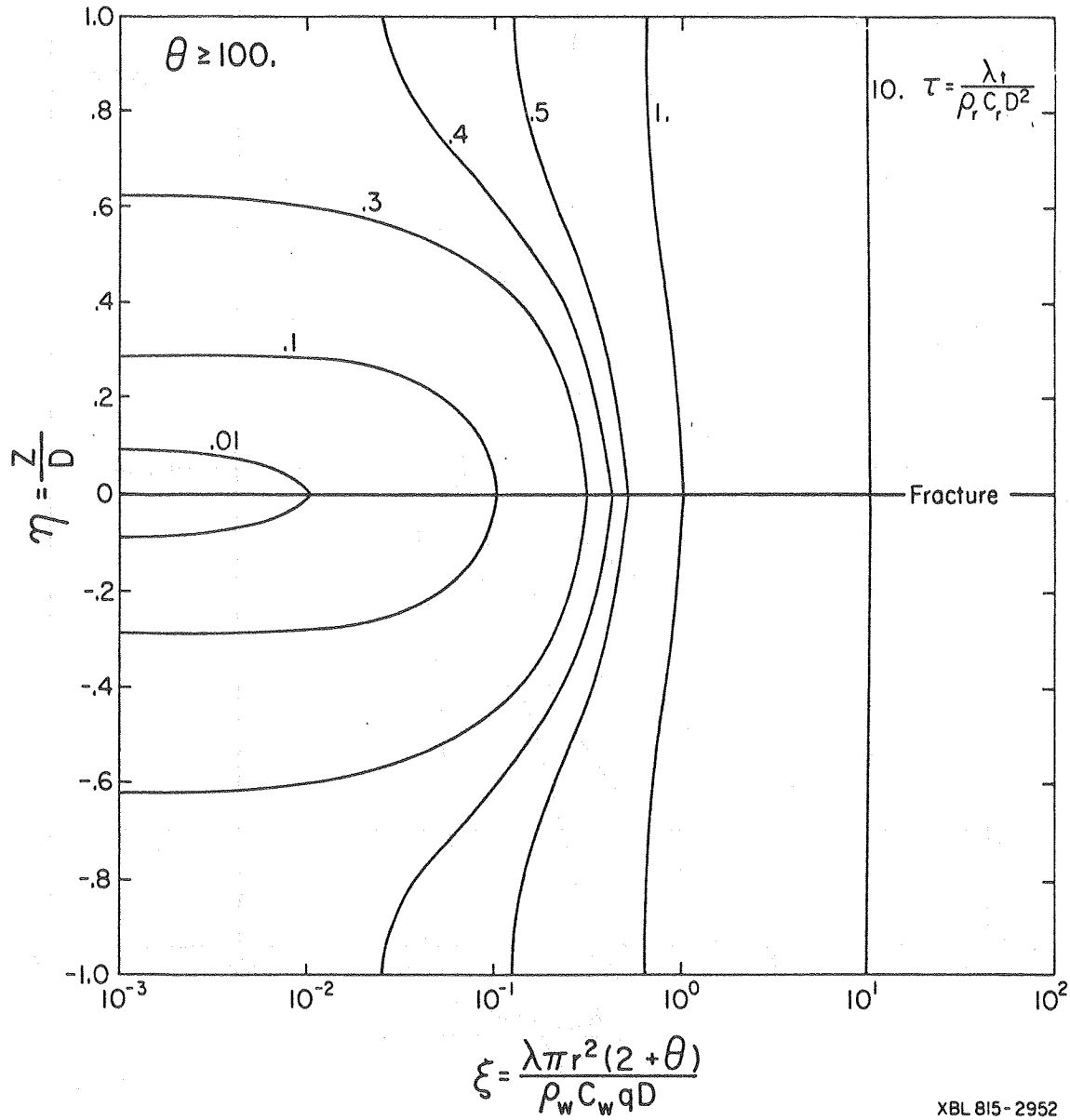
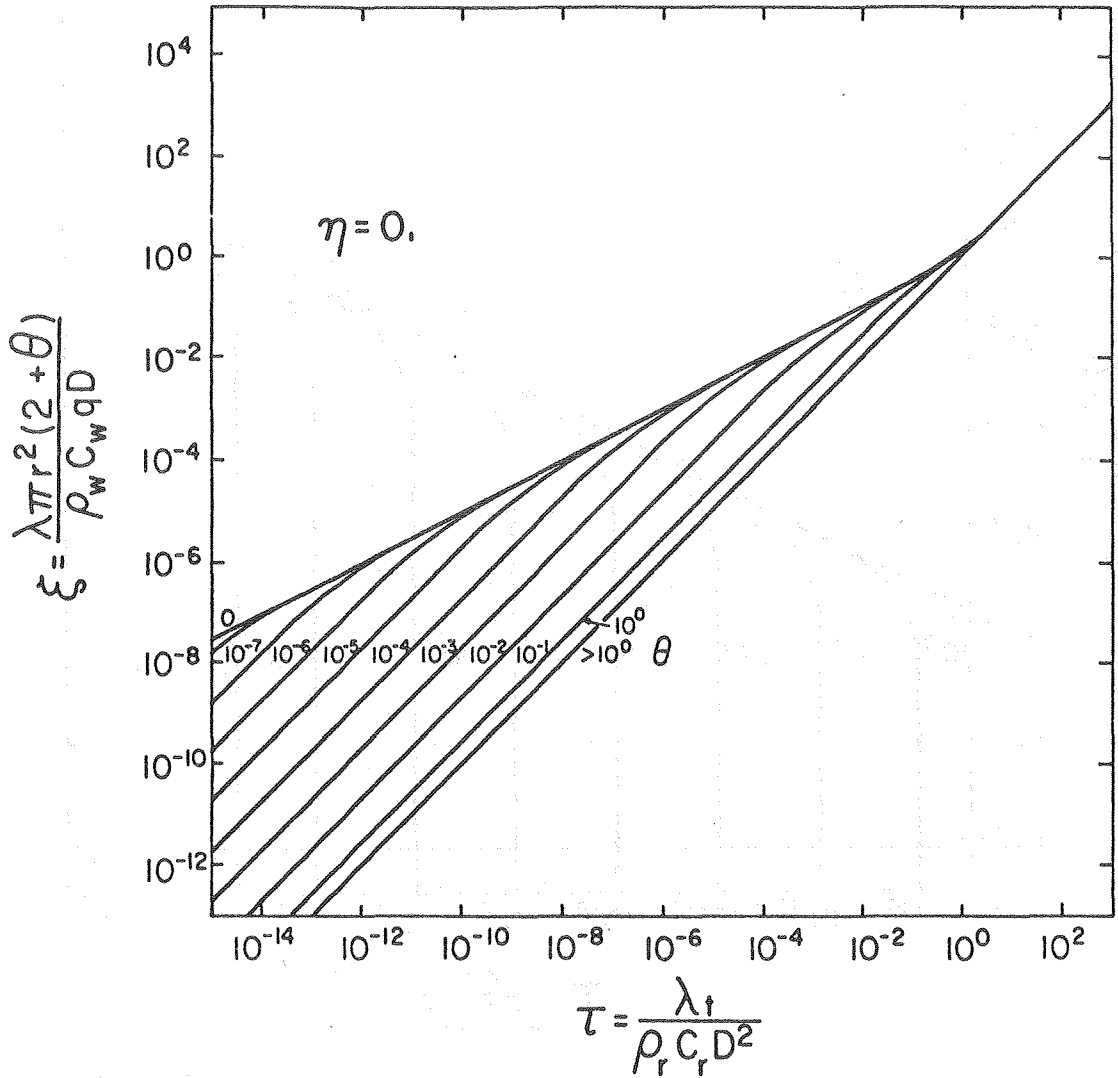
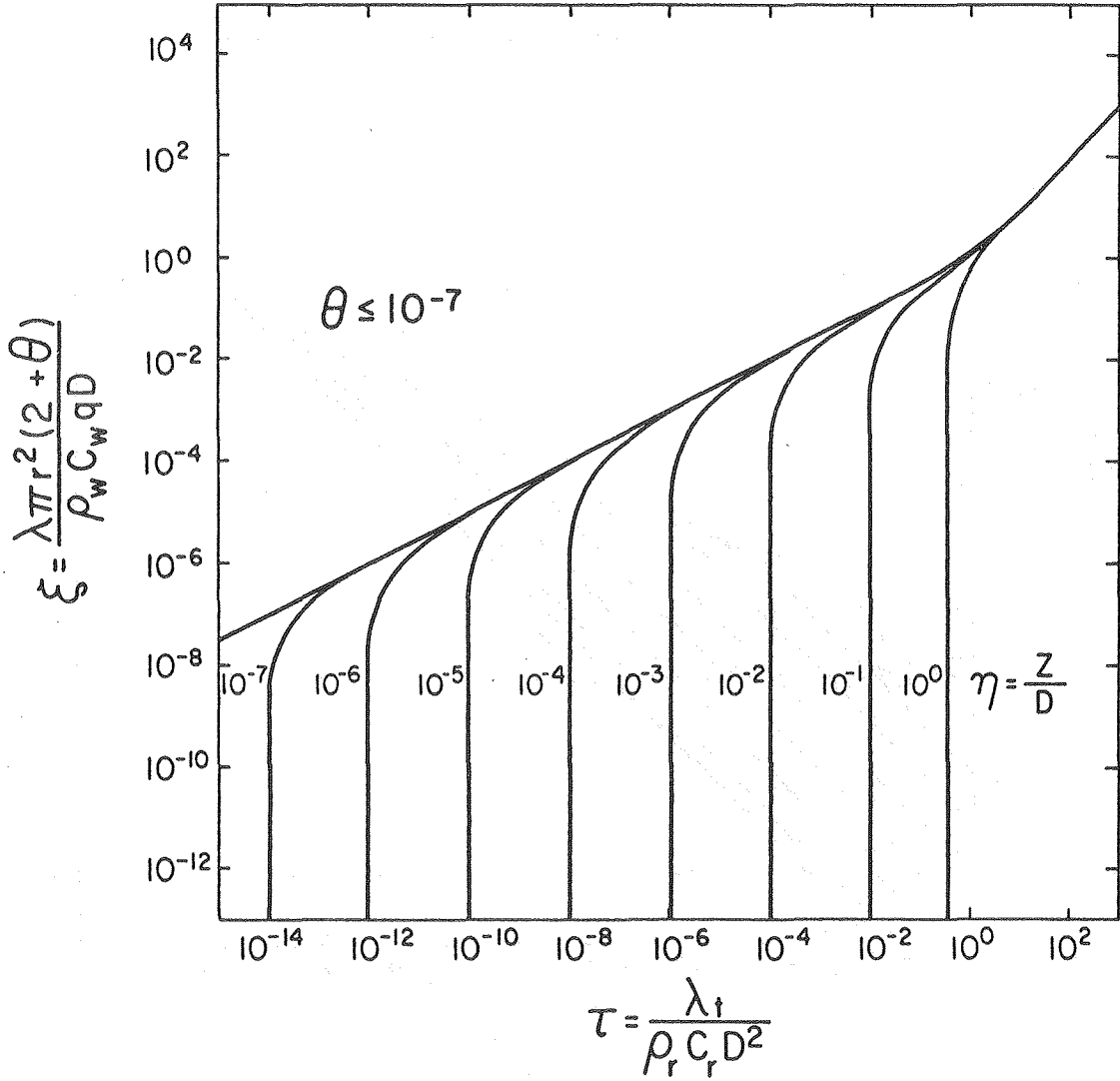


Figure 4



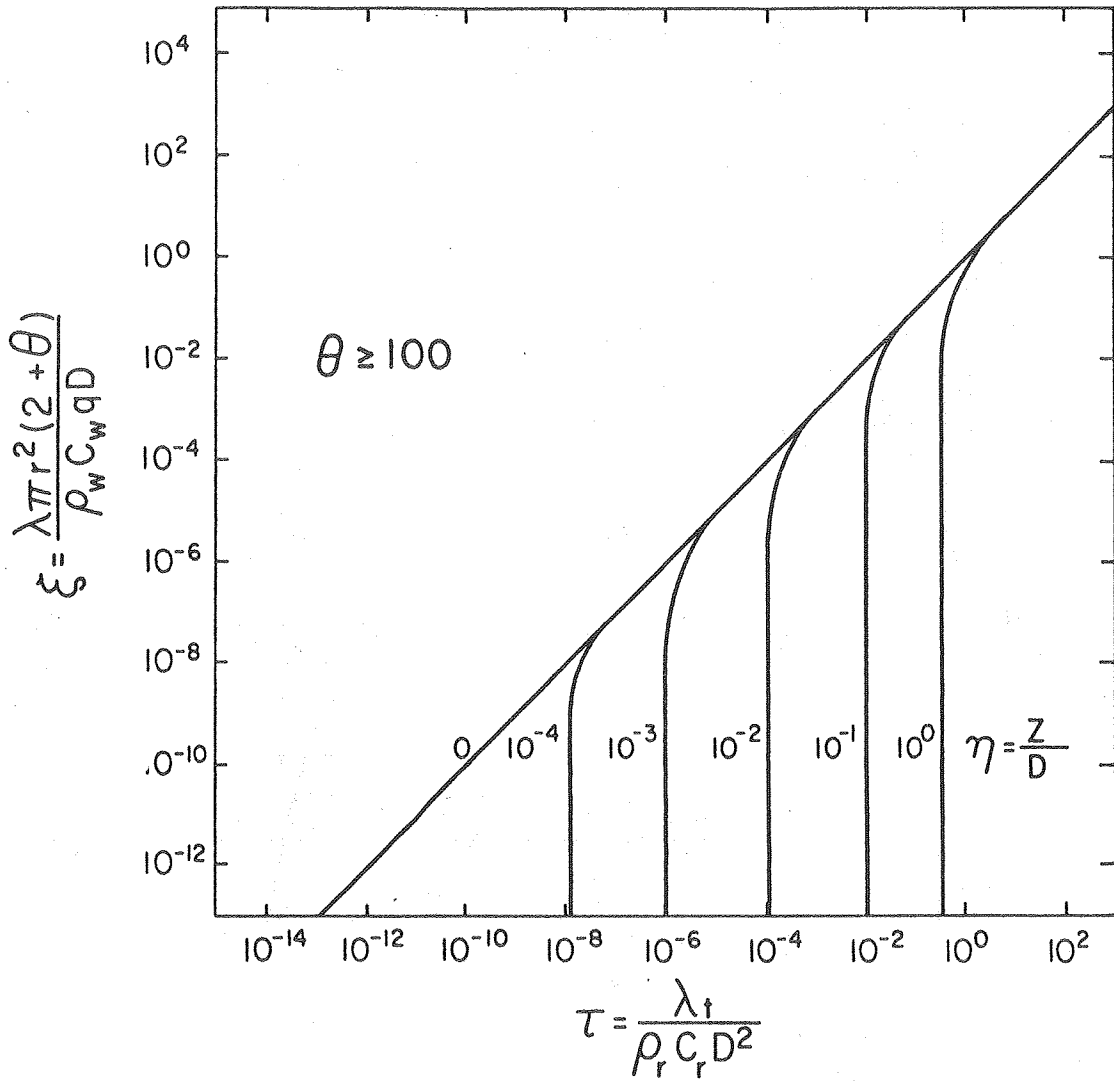
XBL 815-2950A

Figure 5



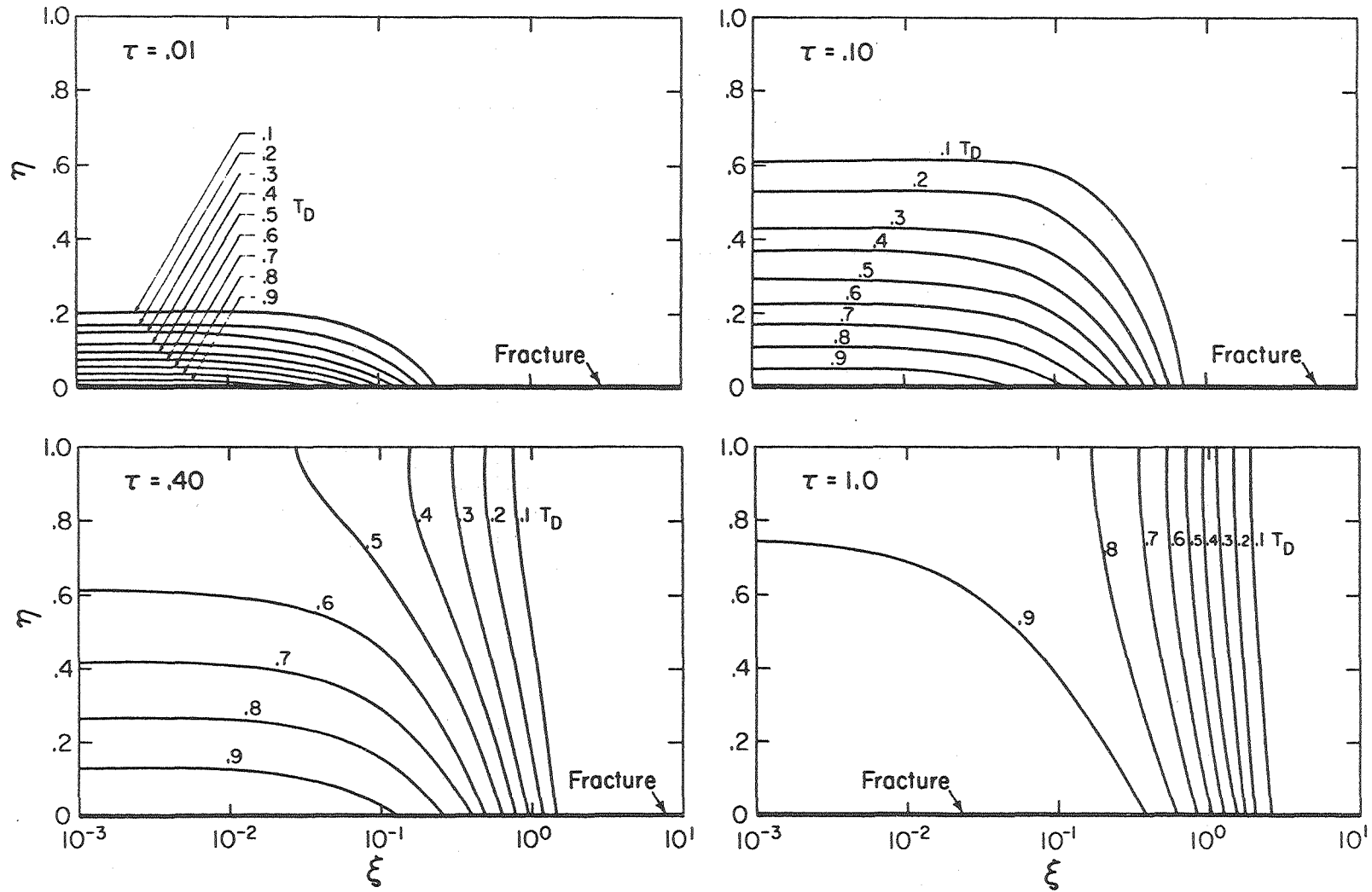
XBL 815-2949

Figure 6



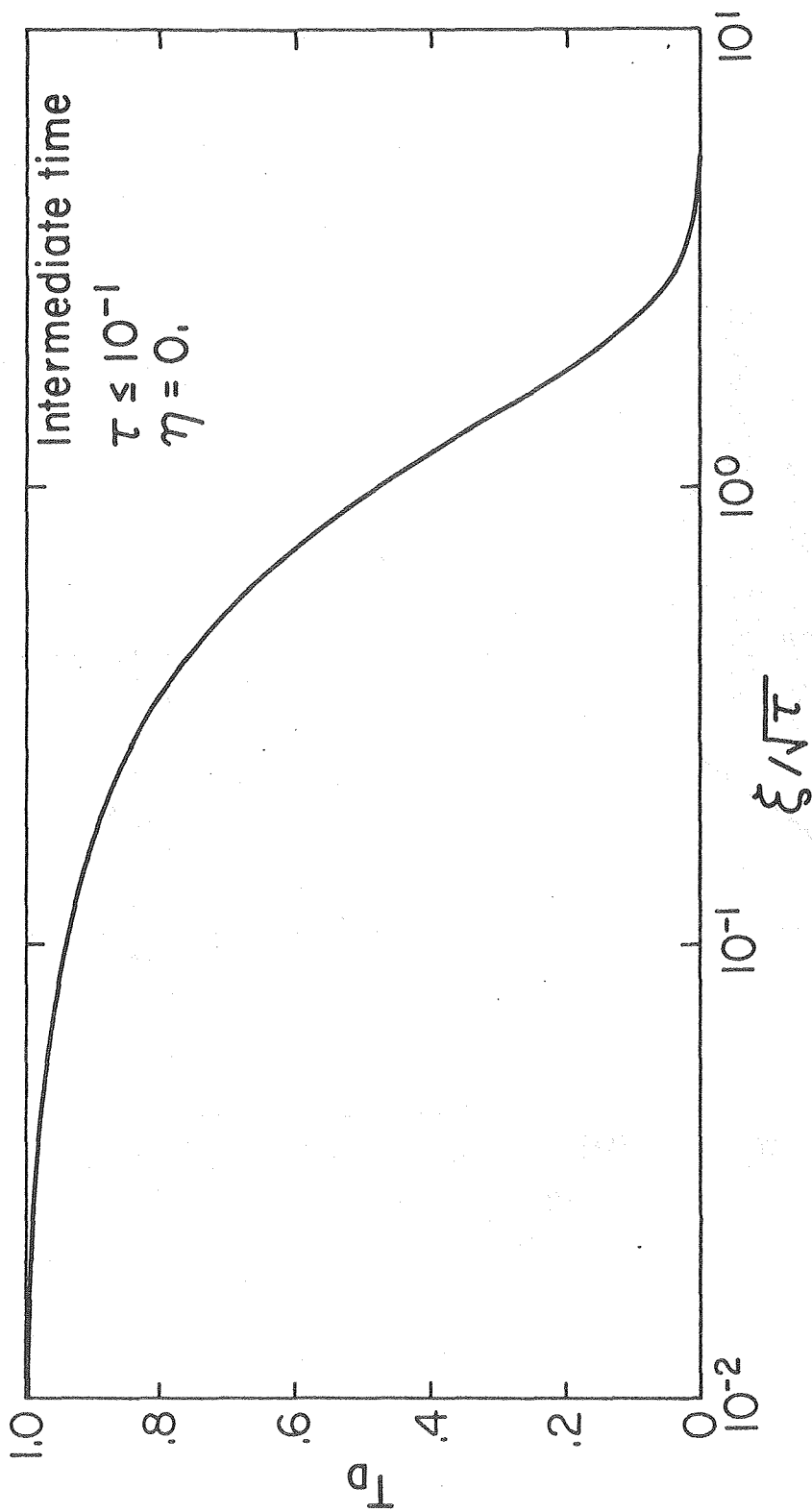
XBL 815-2948

Figure 7



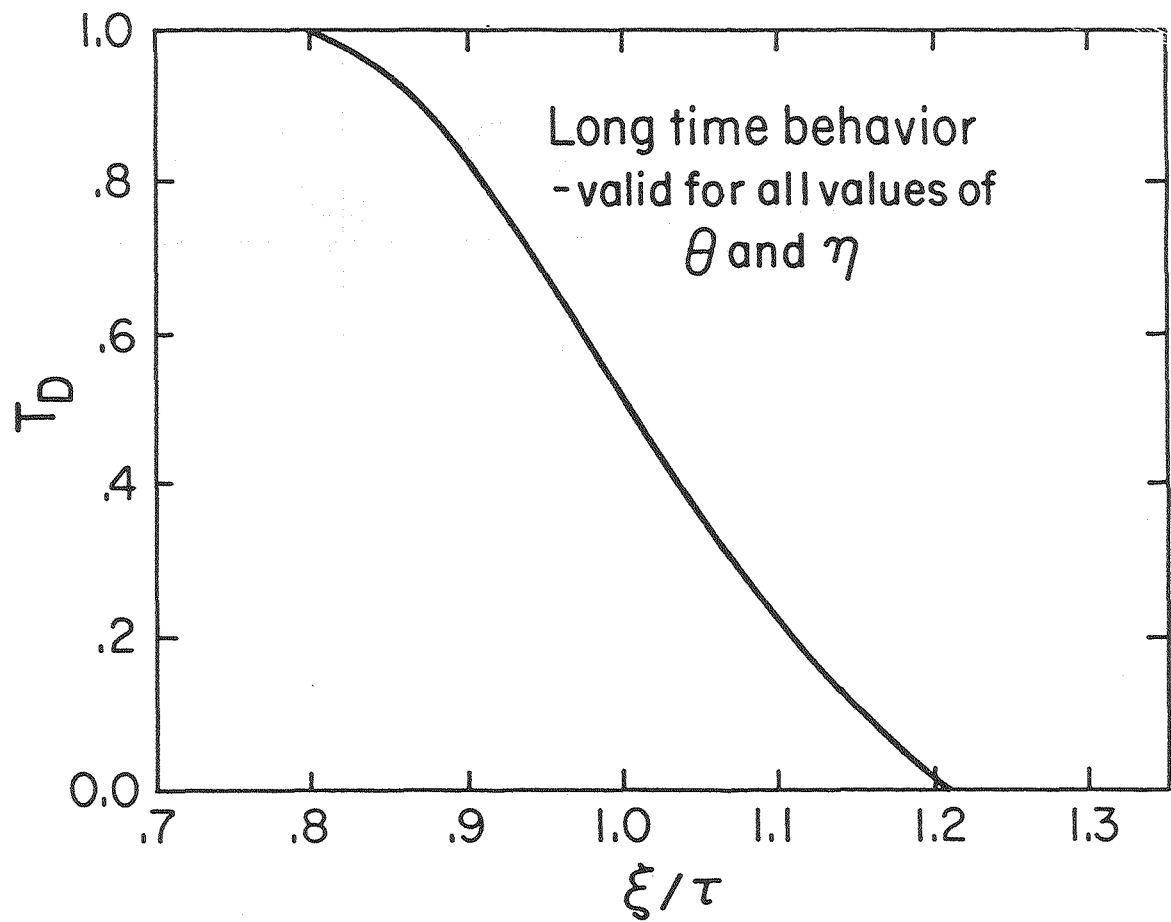
XBL 815-2953

Figure 8



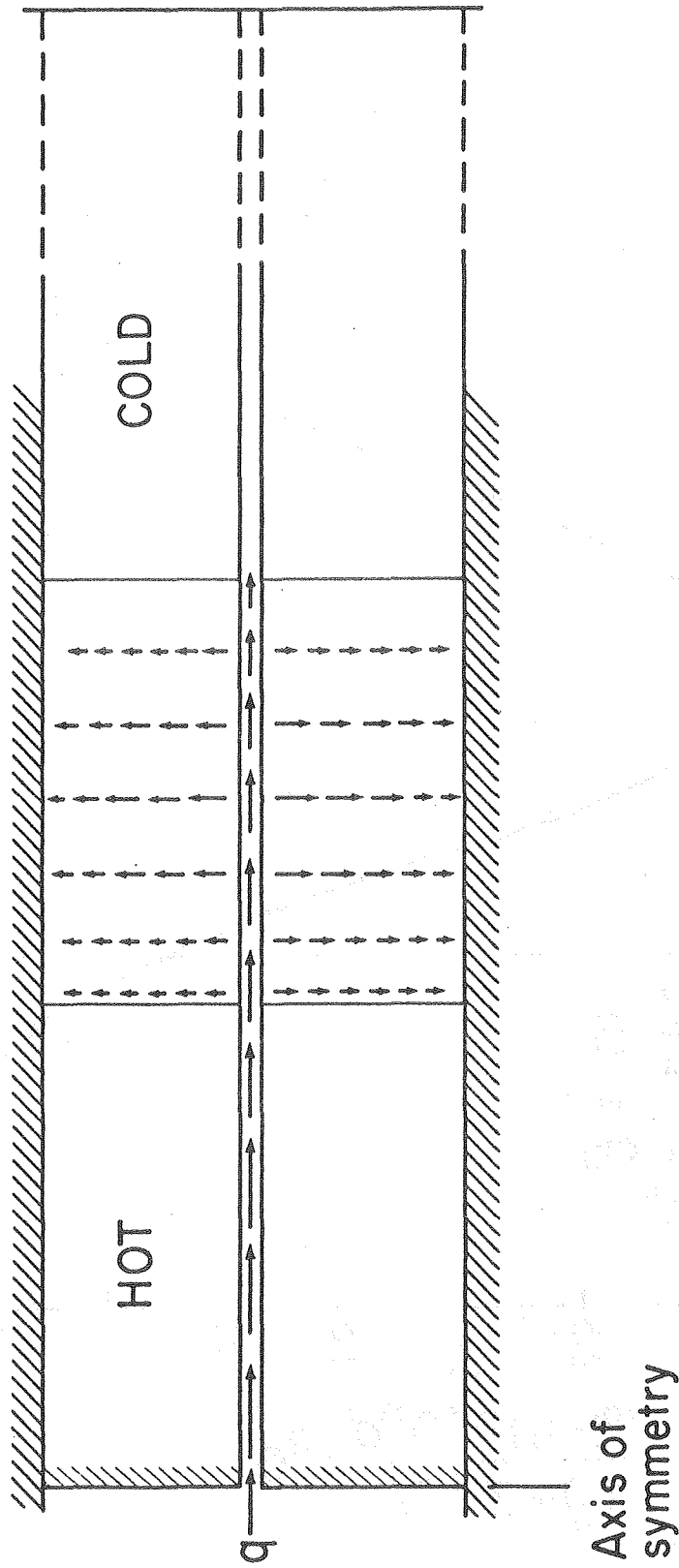
XBL 815-2954

Figure 9



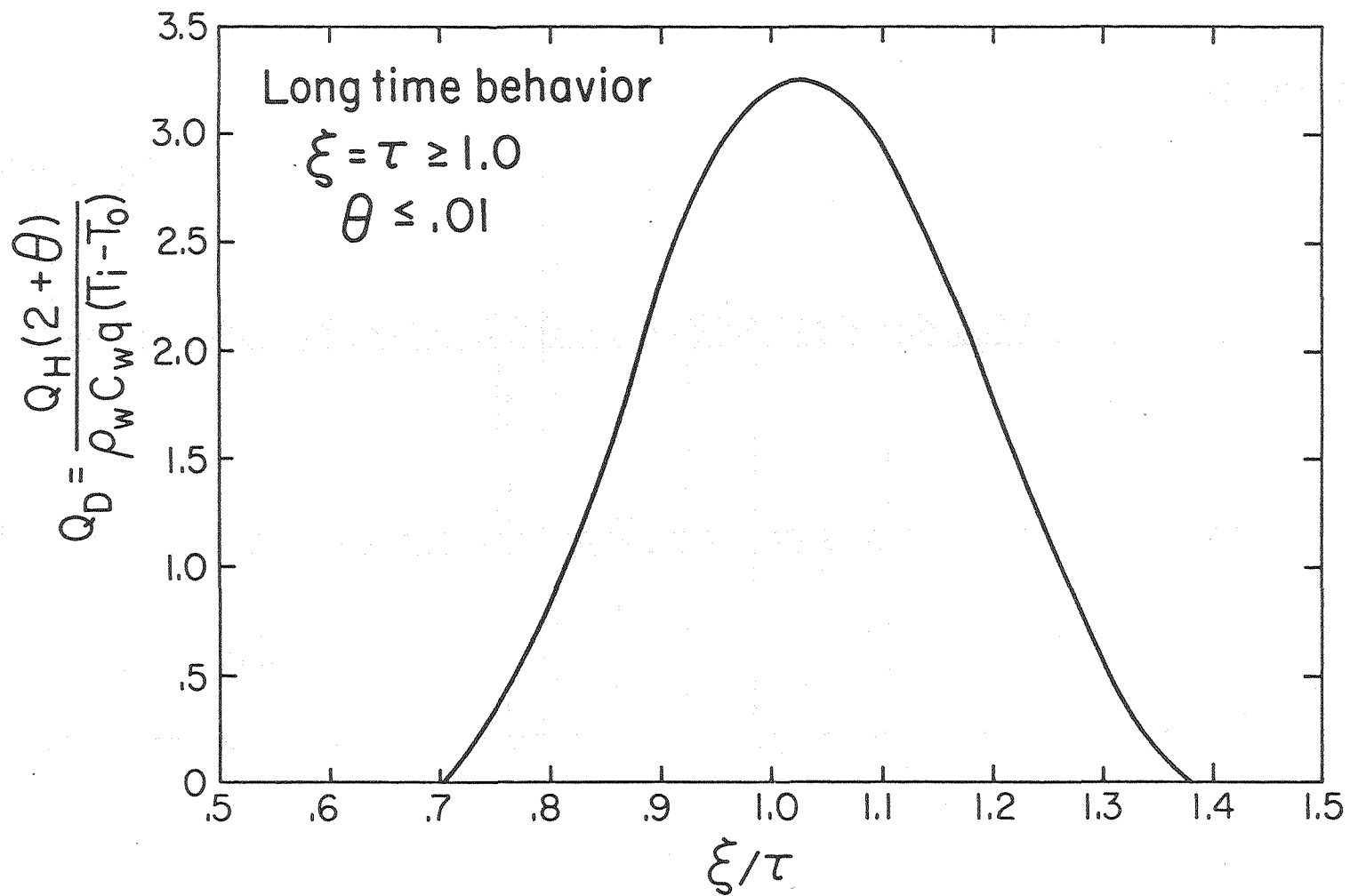
XBL815-2955

Figure 10



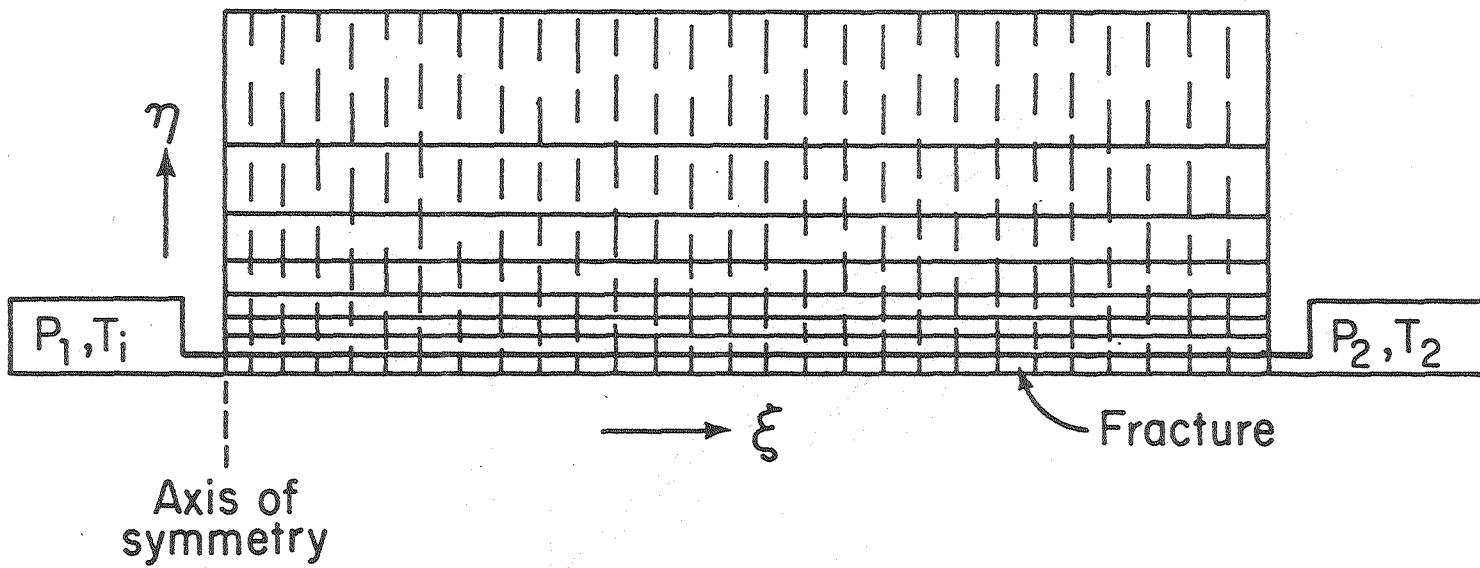
XBL 815 - 2956

Figure 11



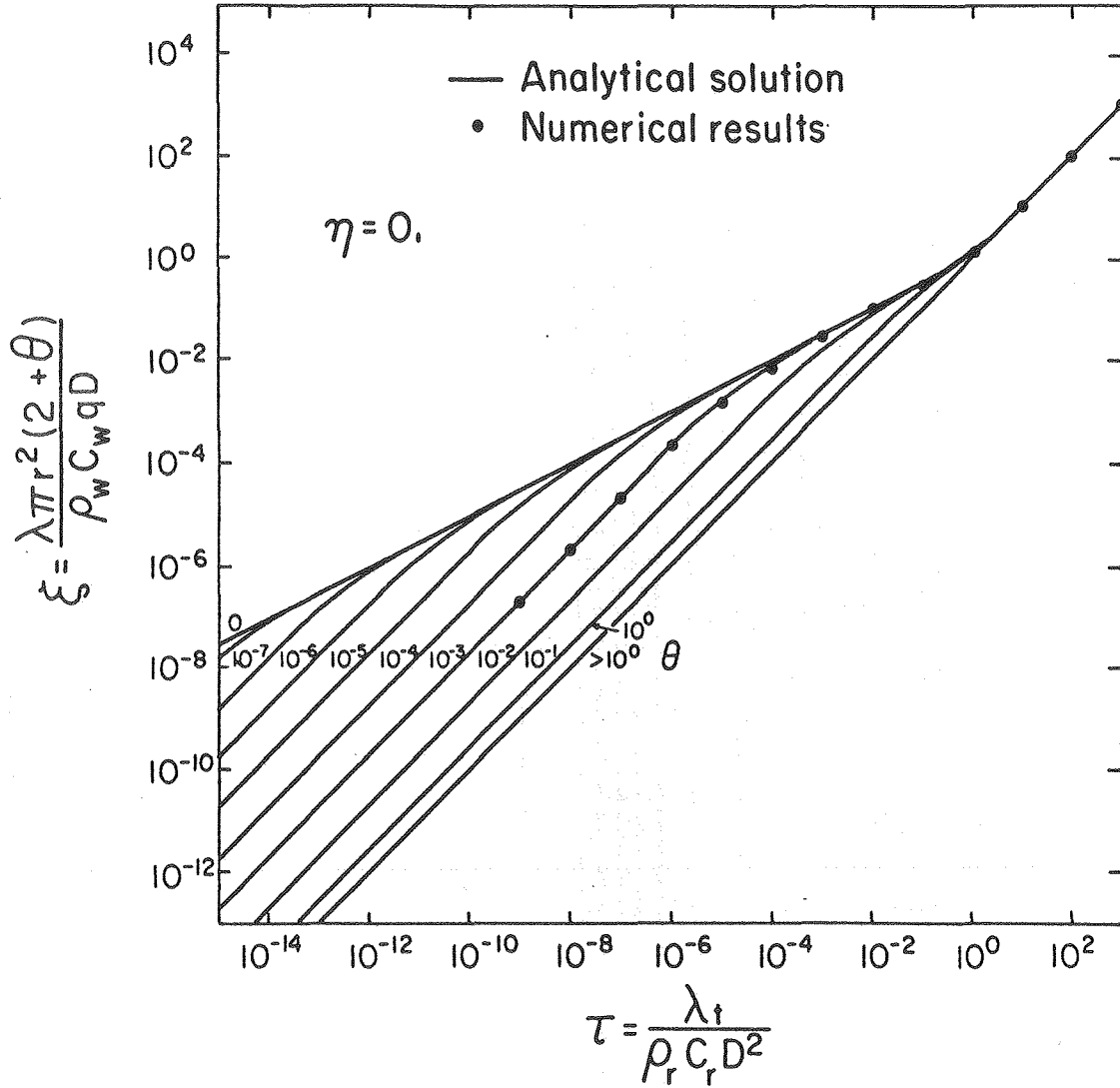
XBL 815-9257

Figure 12



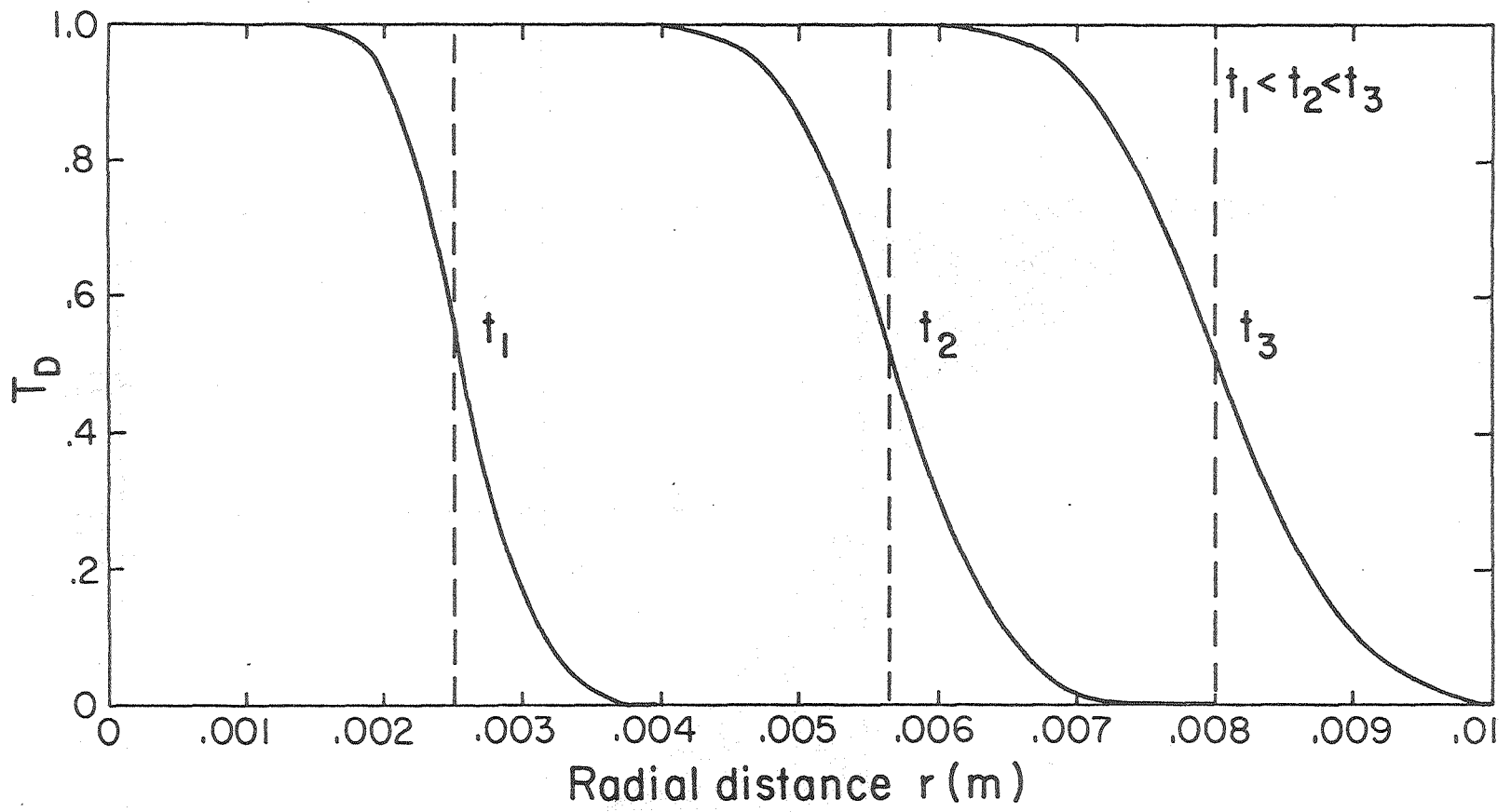
XBL 815-2958

Figure 13



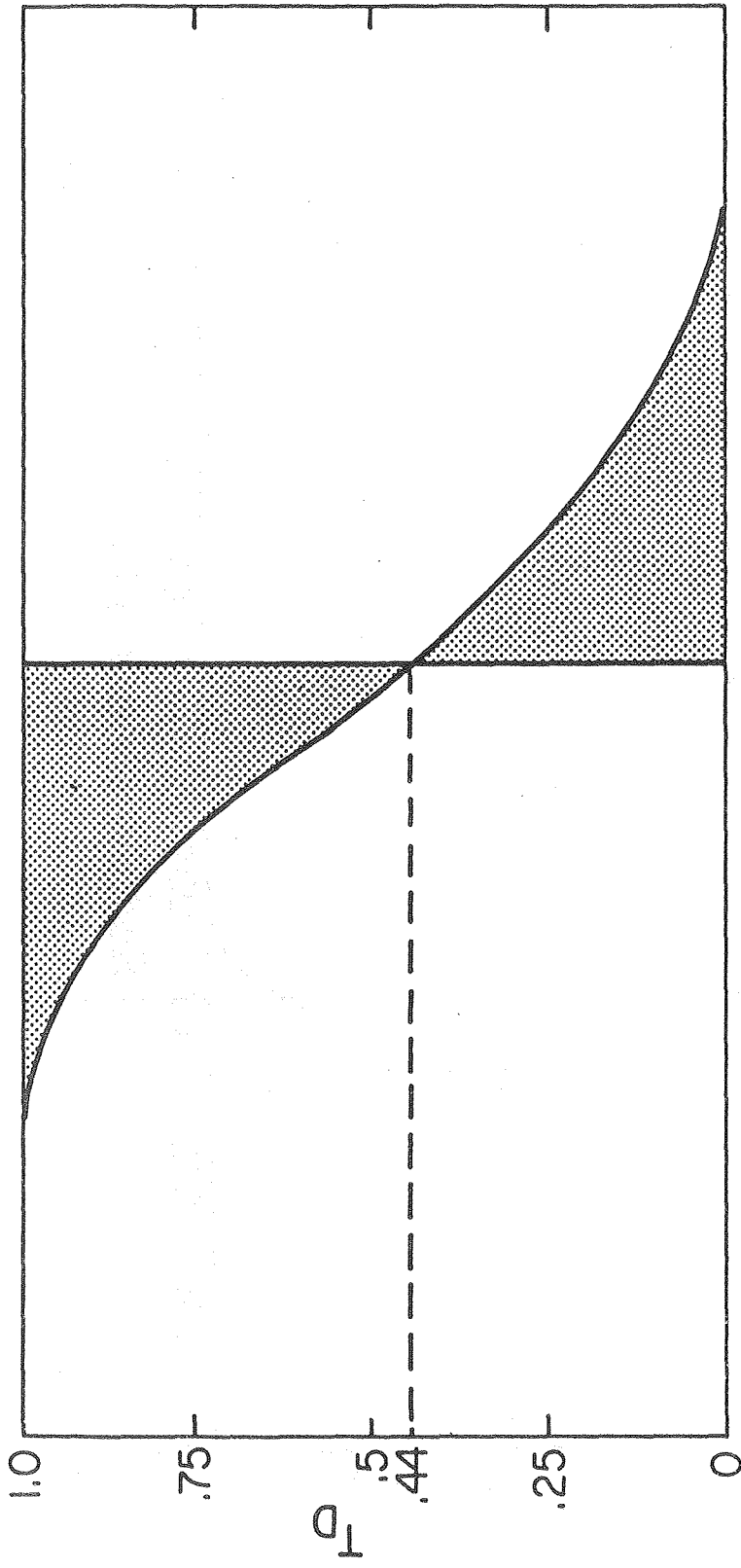
XBL 815-2950

Figure 14



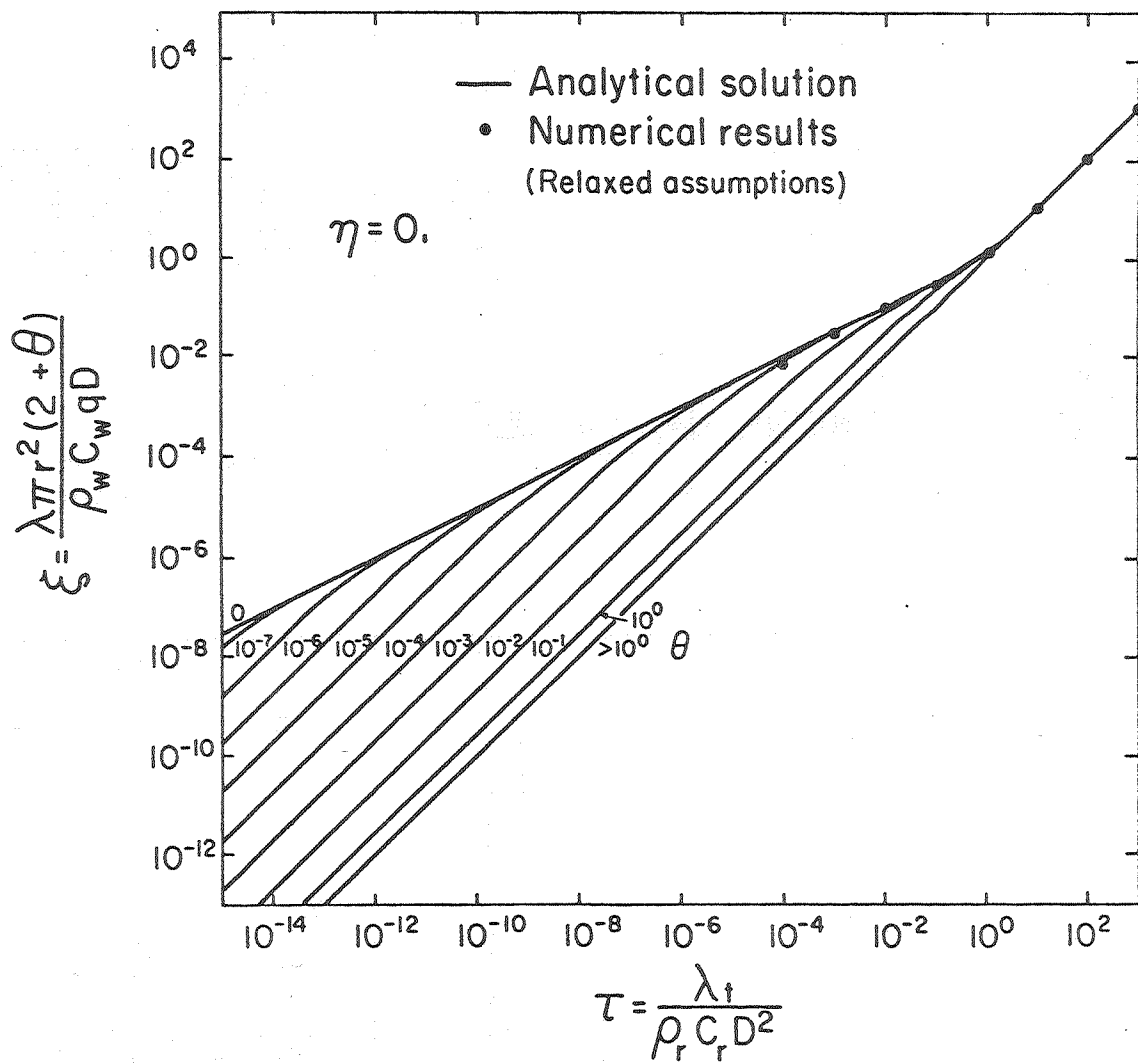
XBL 815-2960

Figure 15



XBL 815-2961

Figure 16



XBL 815-2967

Figure 17

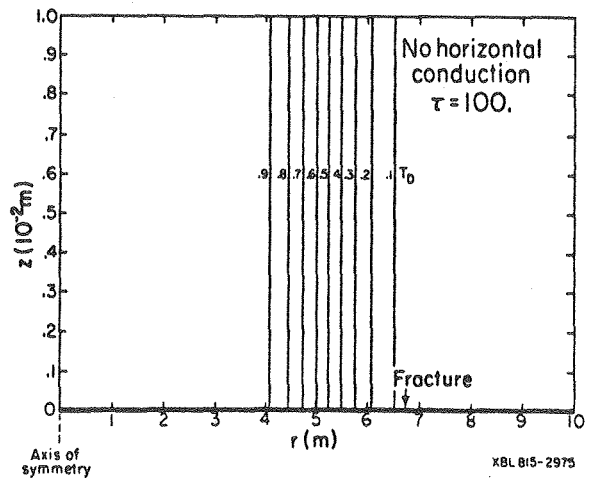
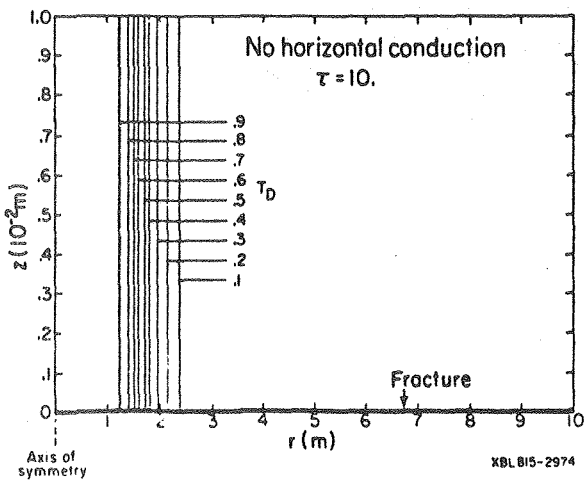
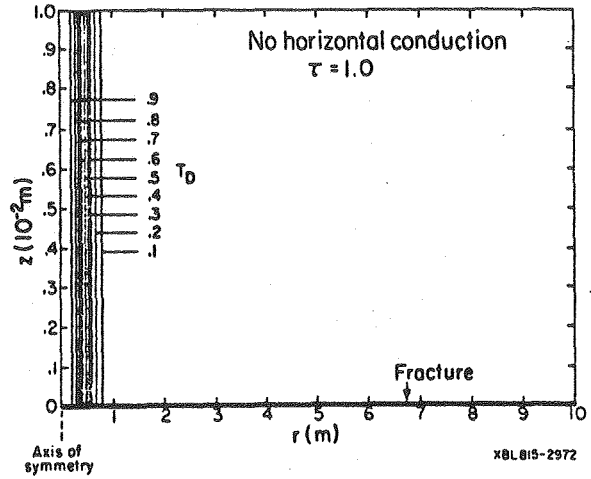
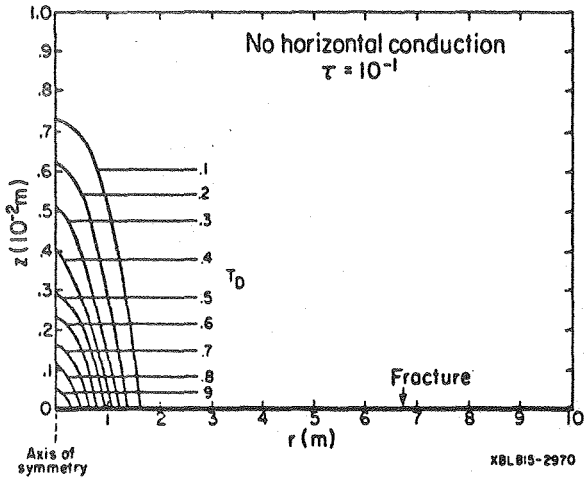
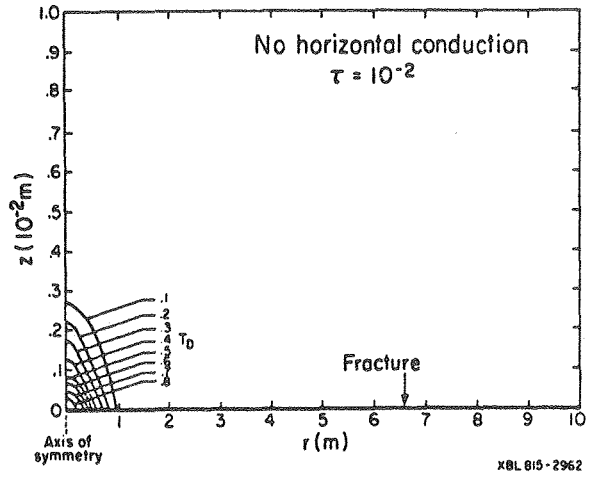
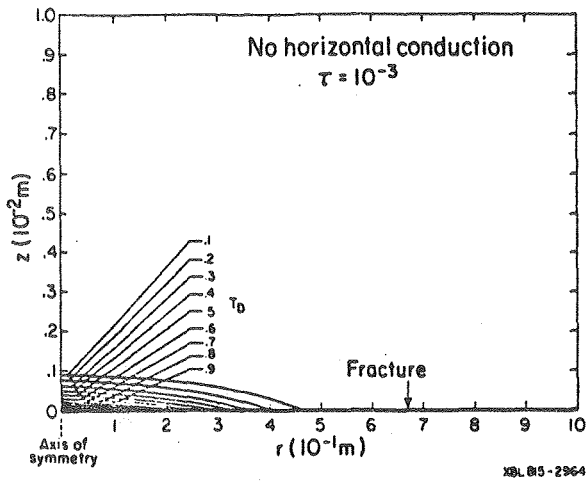


Figure 18

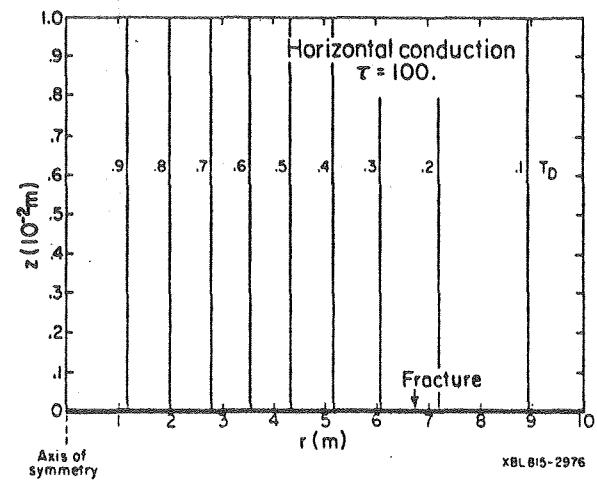
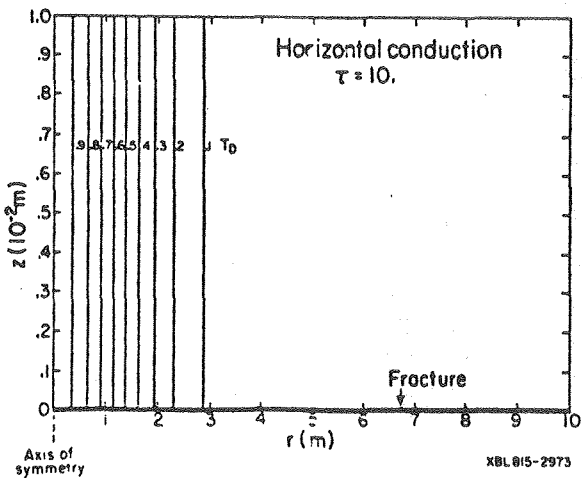
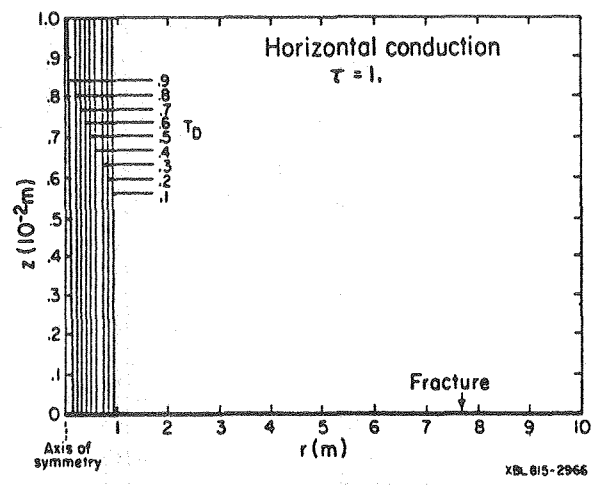
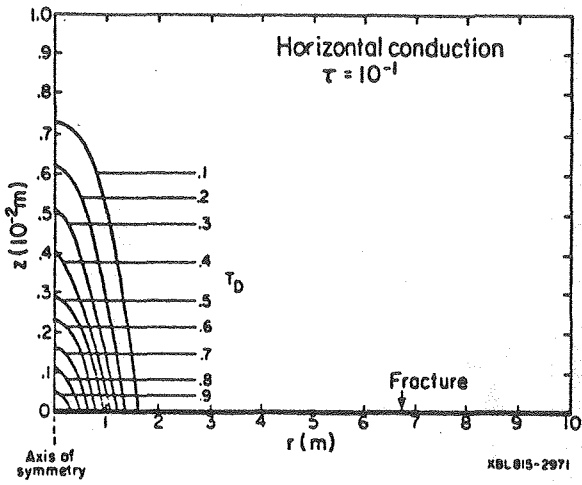
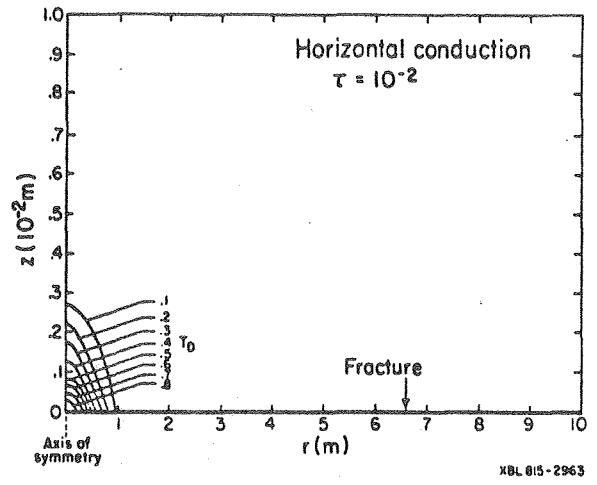
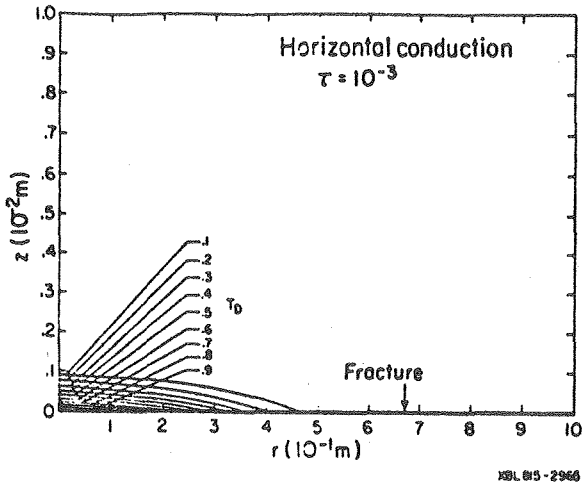
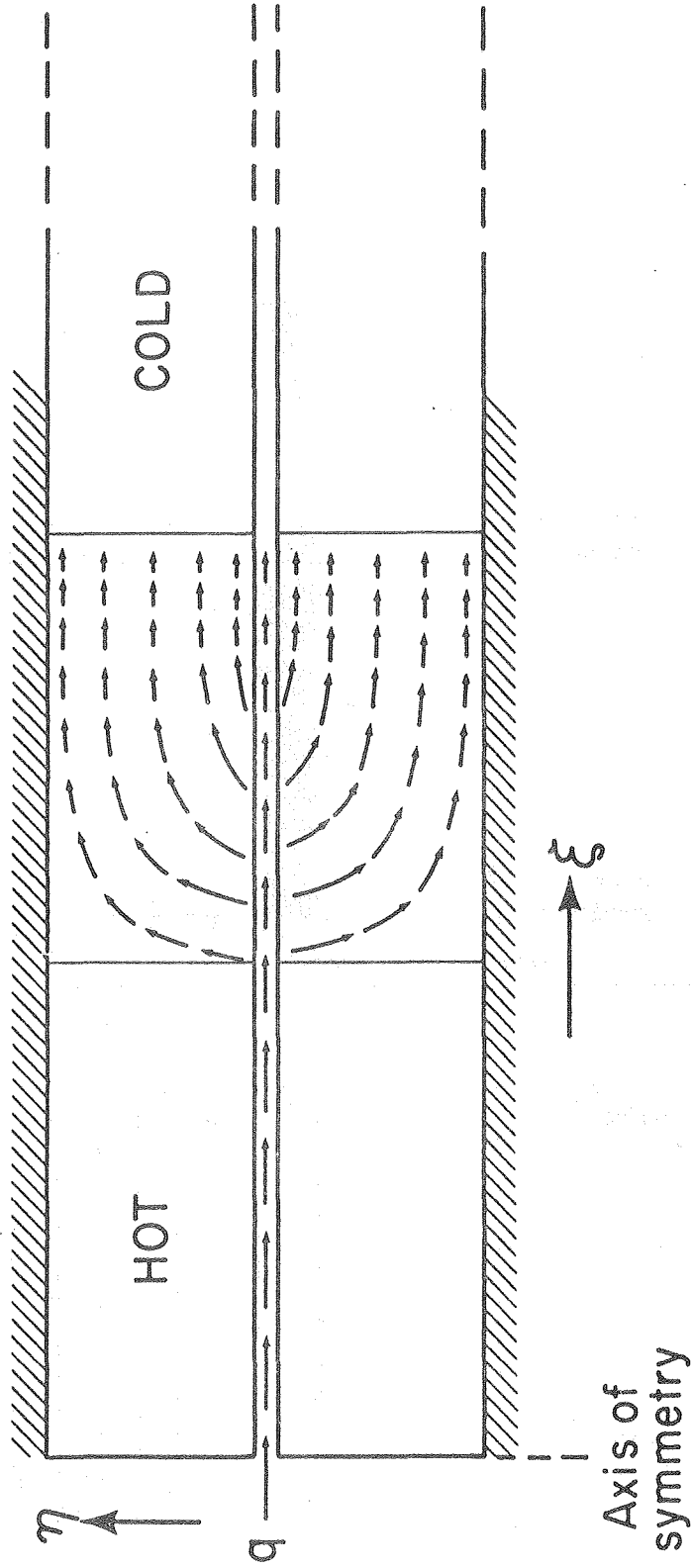
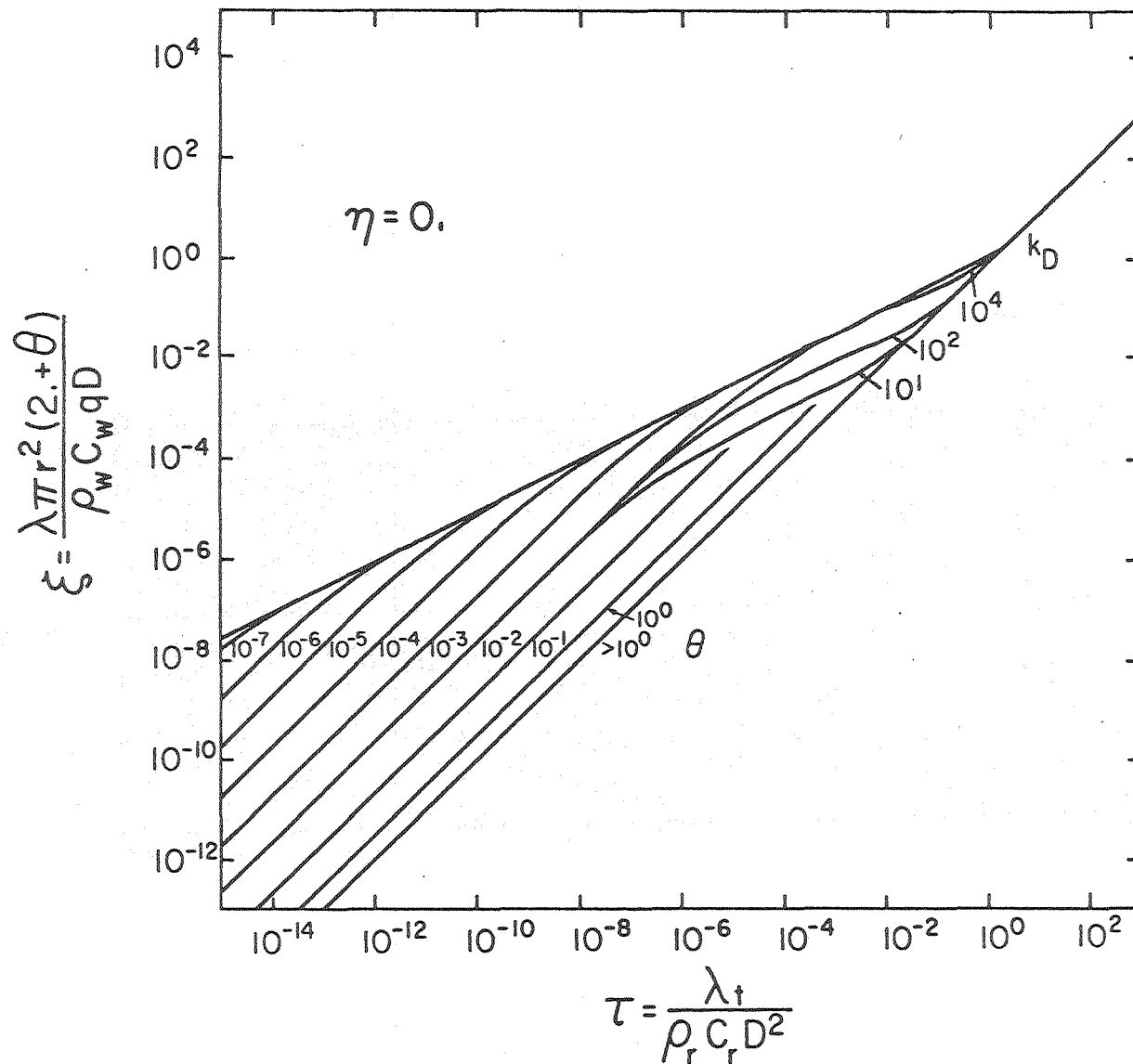


Figure 19



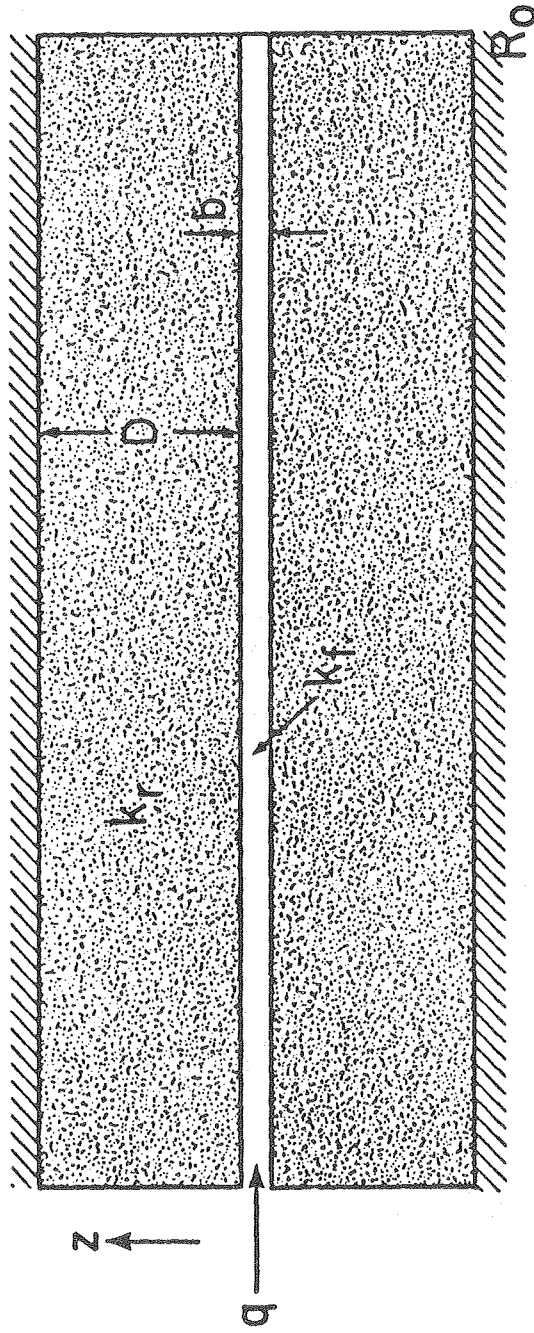
XBL 815-2977

Figure 20



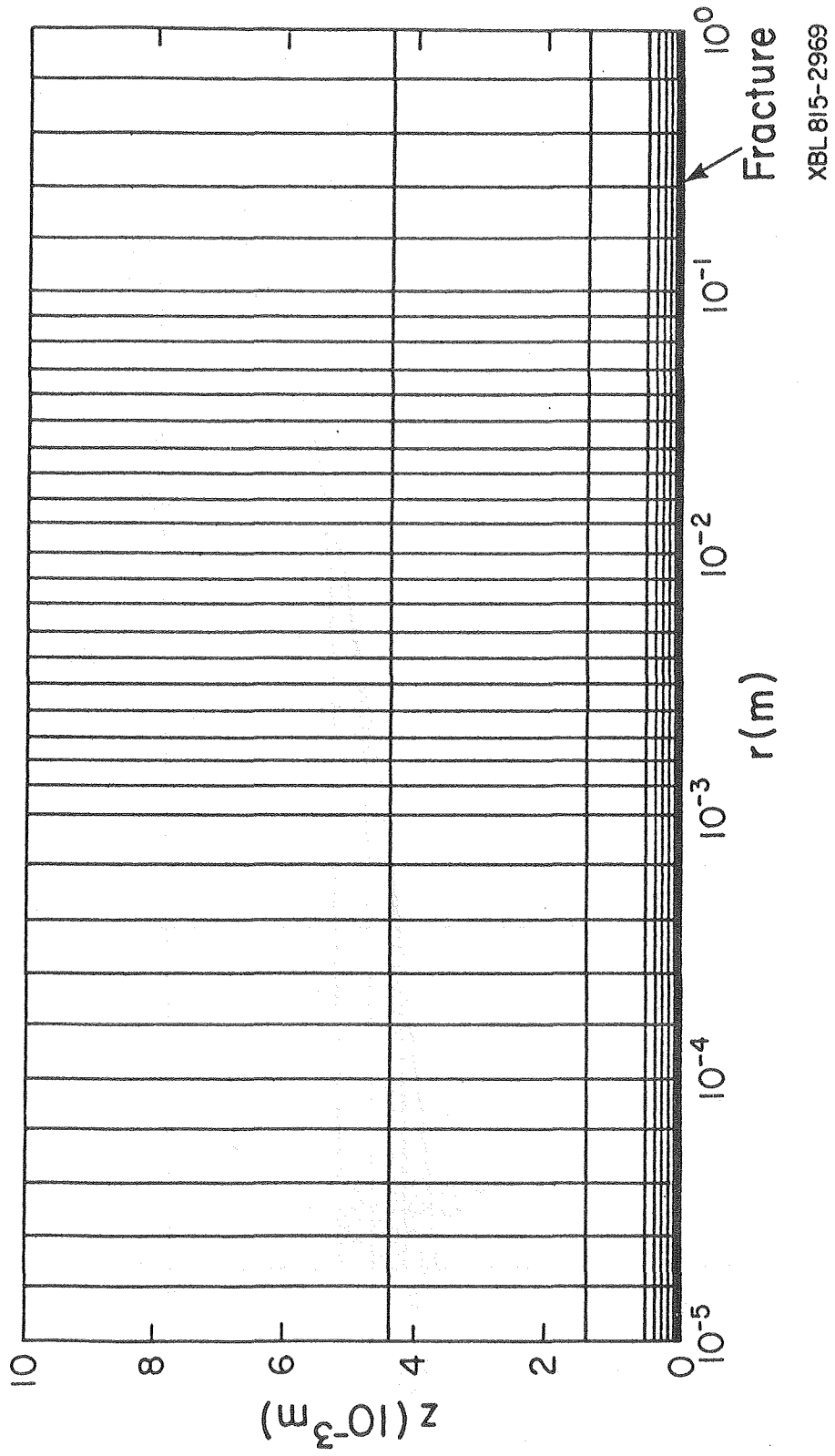
XBL 815-2984

Figure 21



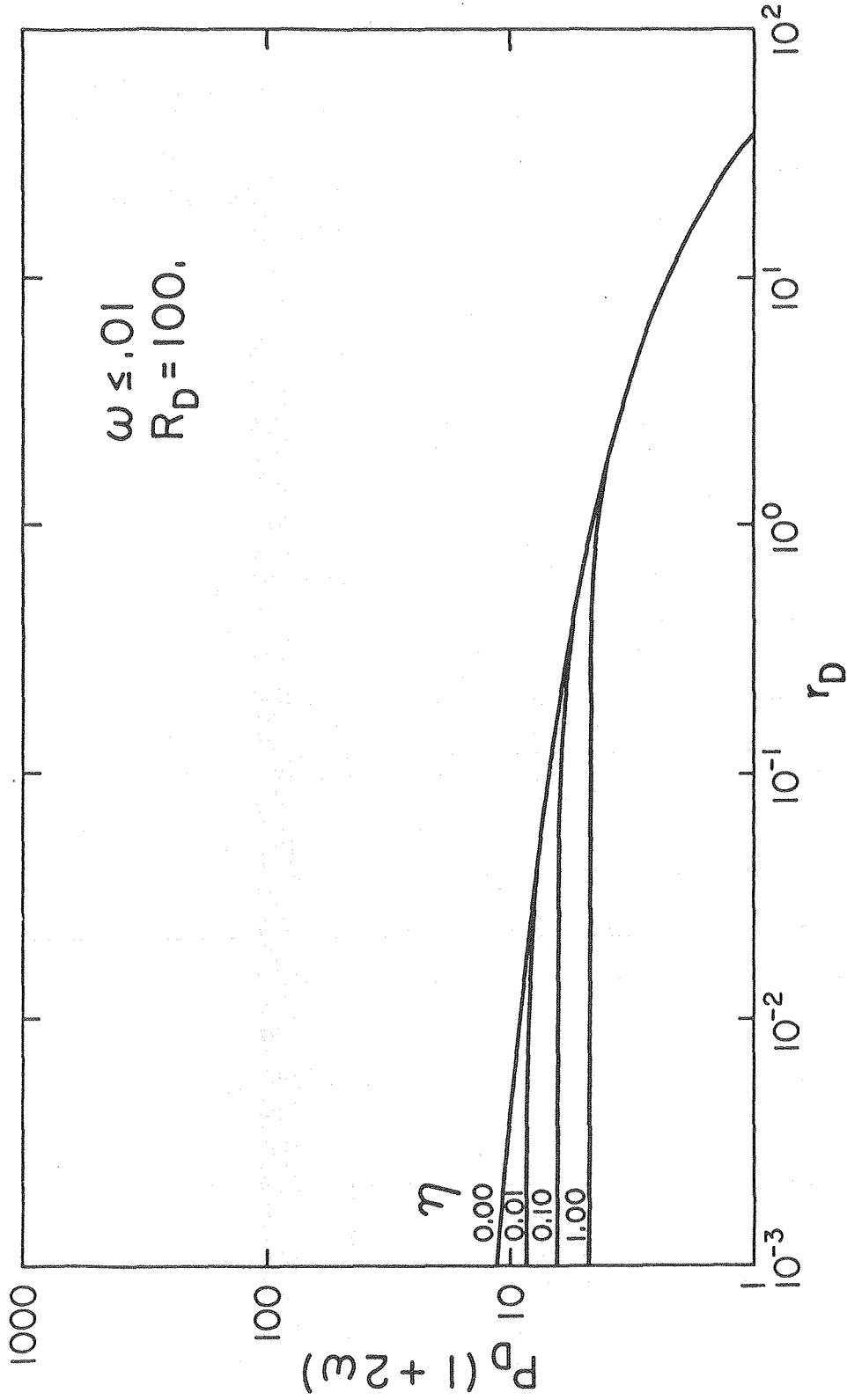
XBL 815-2968

Figure 22



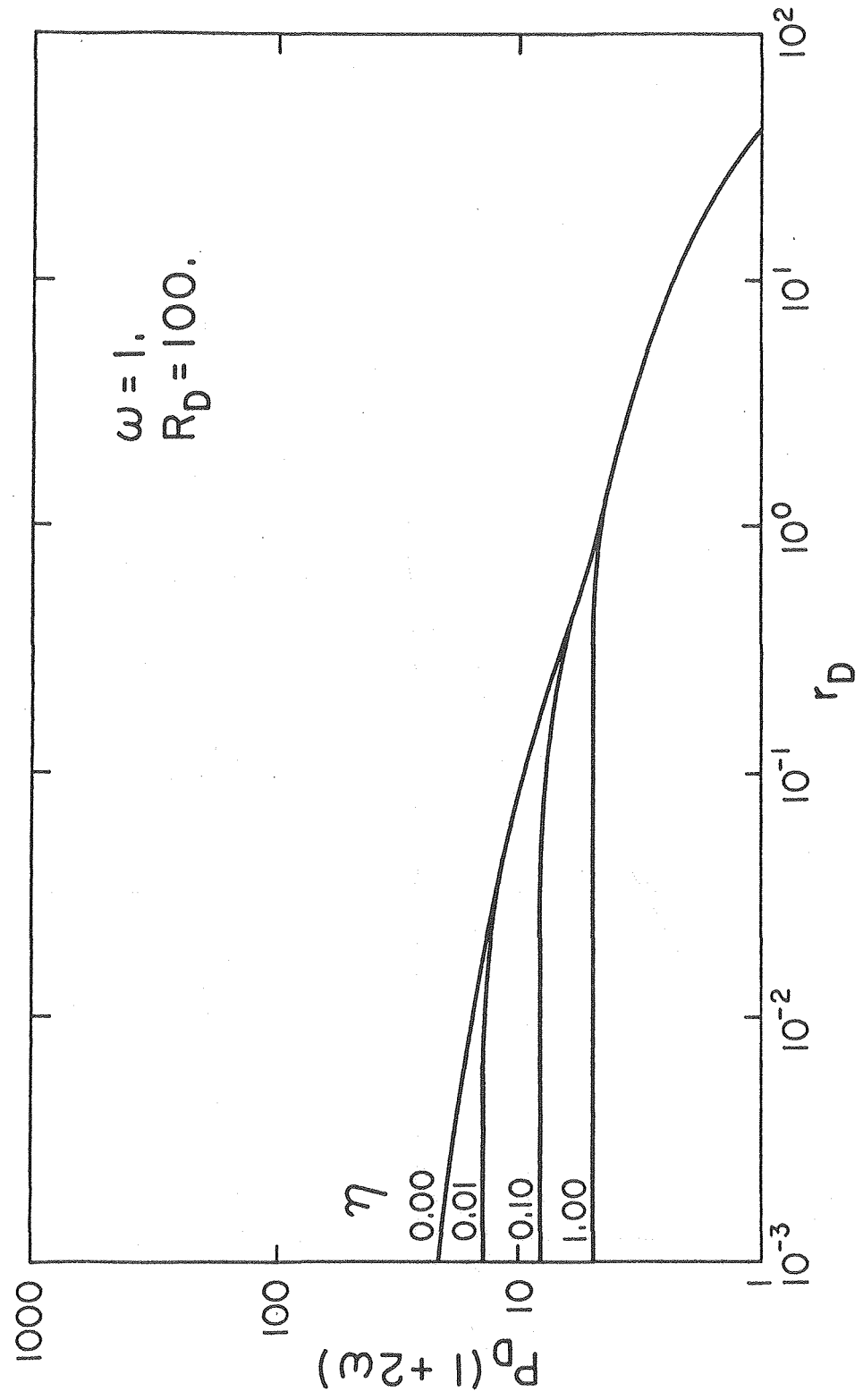
XBL 815-2969

Figure 23



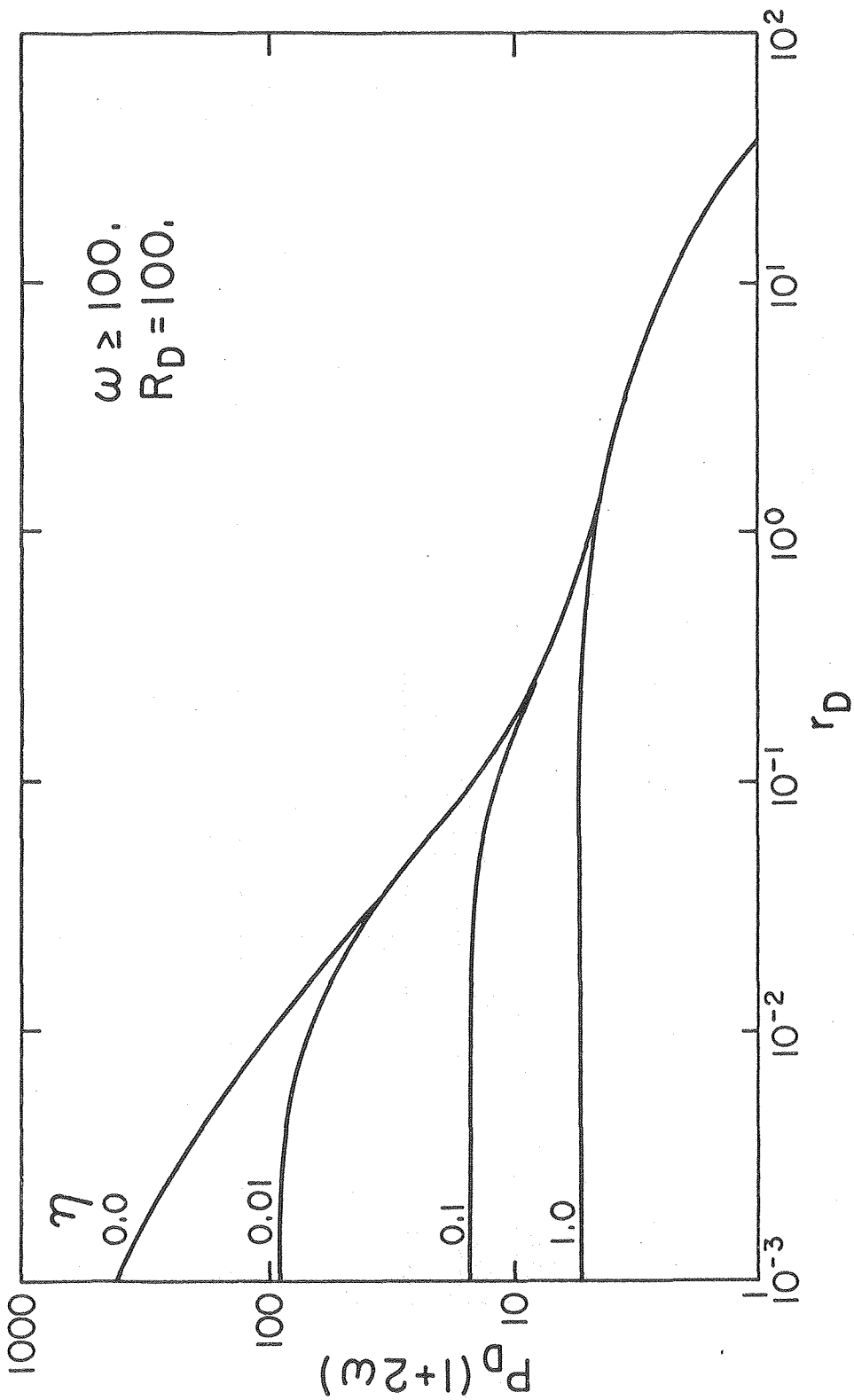
XBL 815-2978

Figure 24



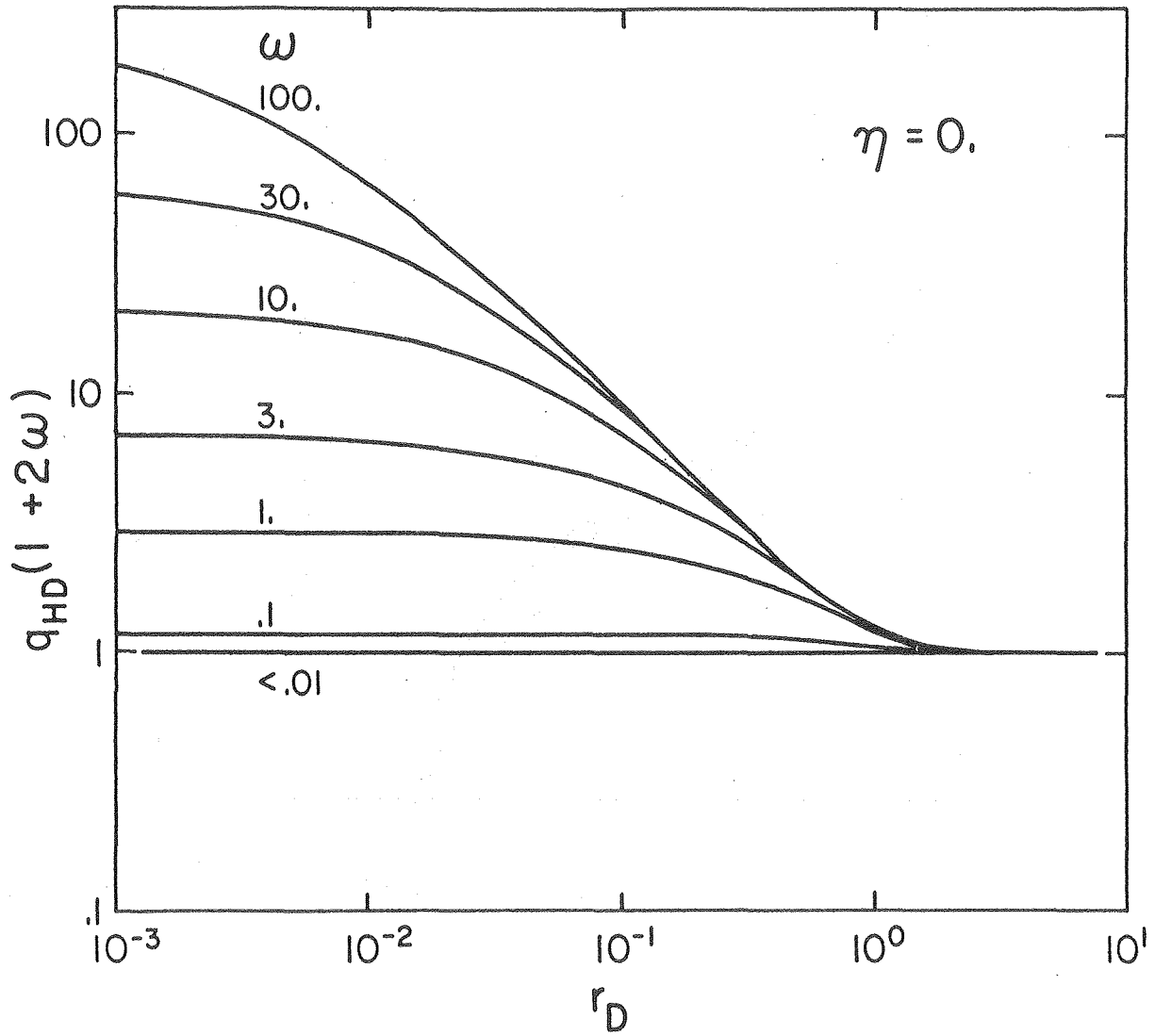
XBL 815-2979

Figure 25



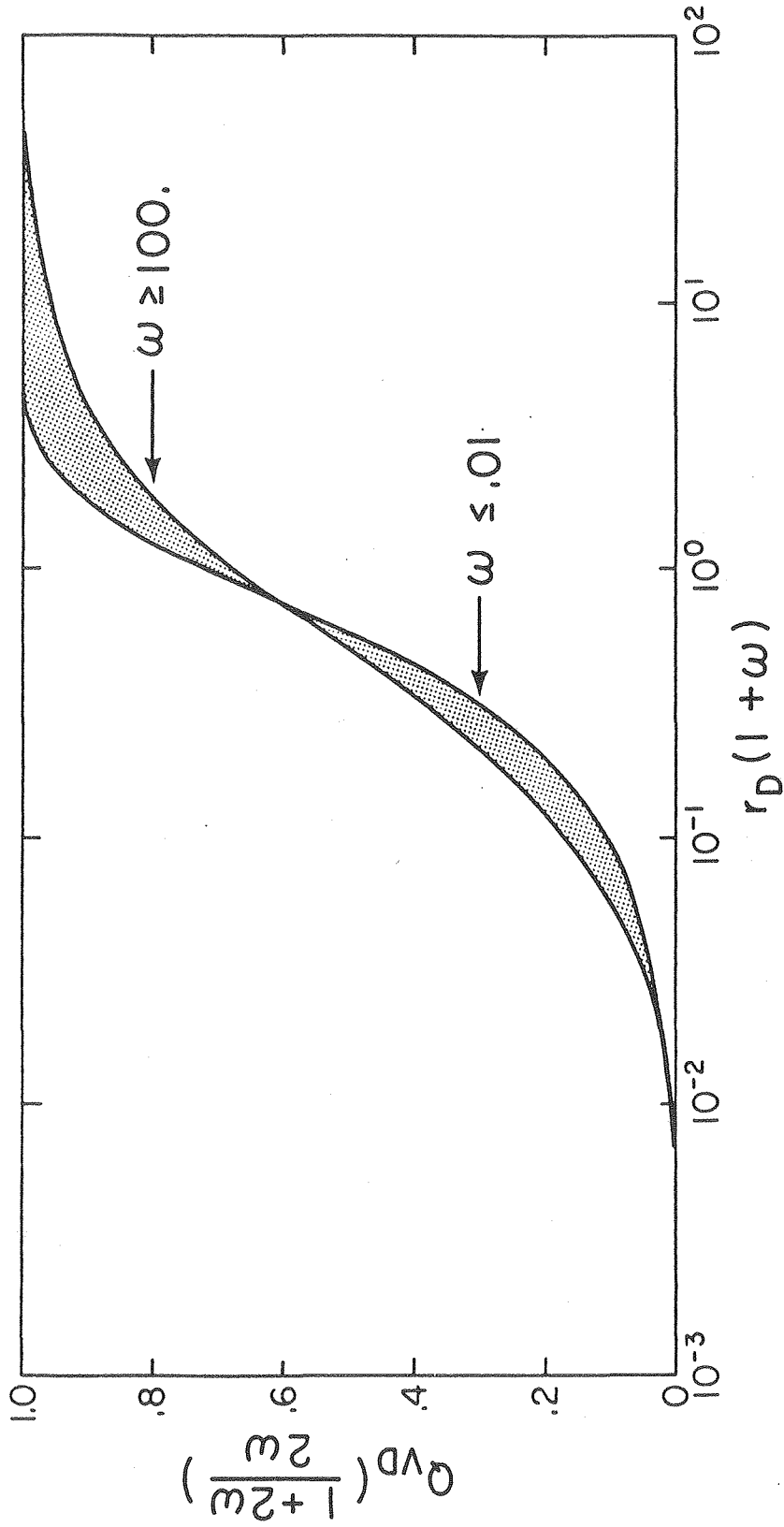
XBL 815 - 2980

Figure 26



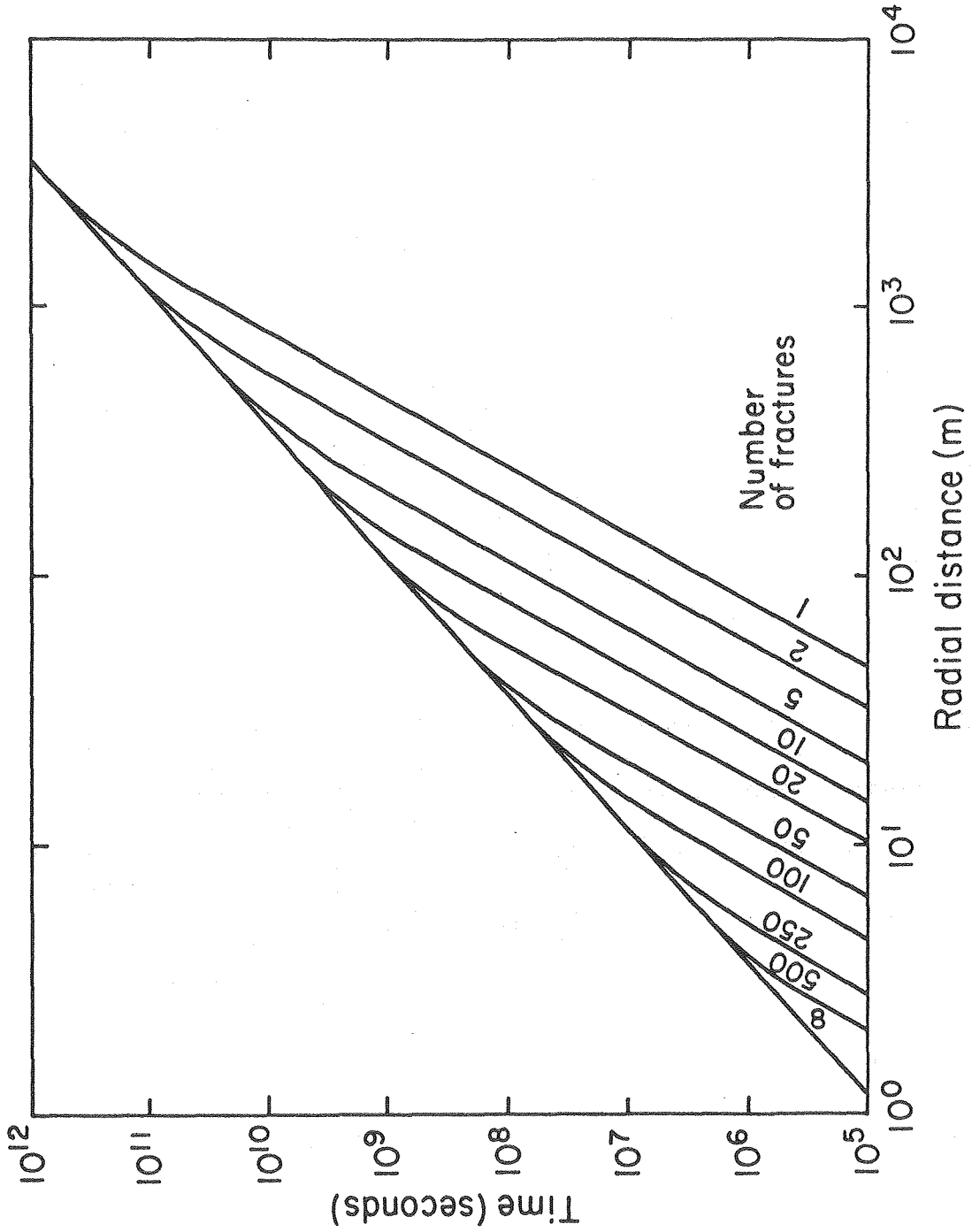
XBL 815-2981

Figure 27



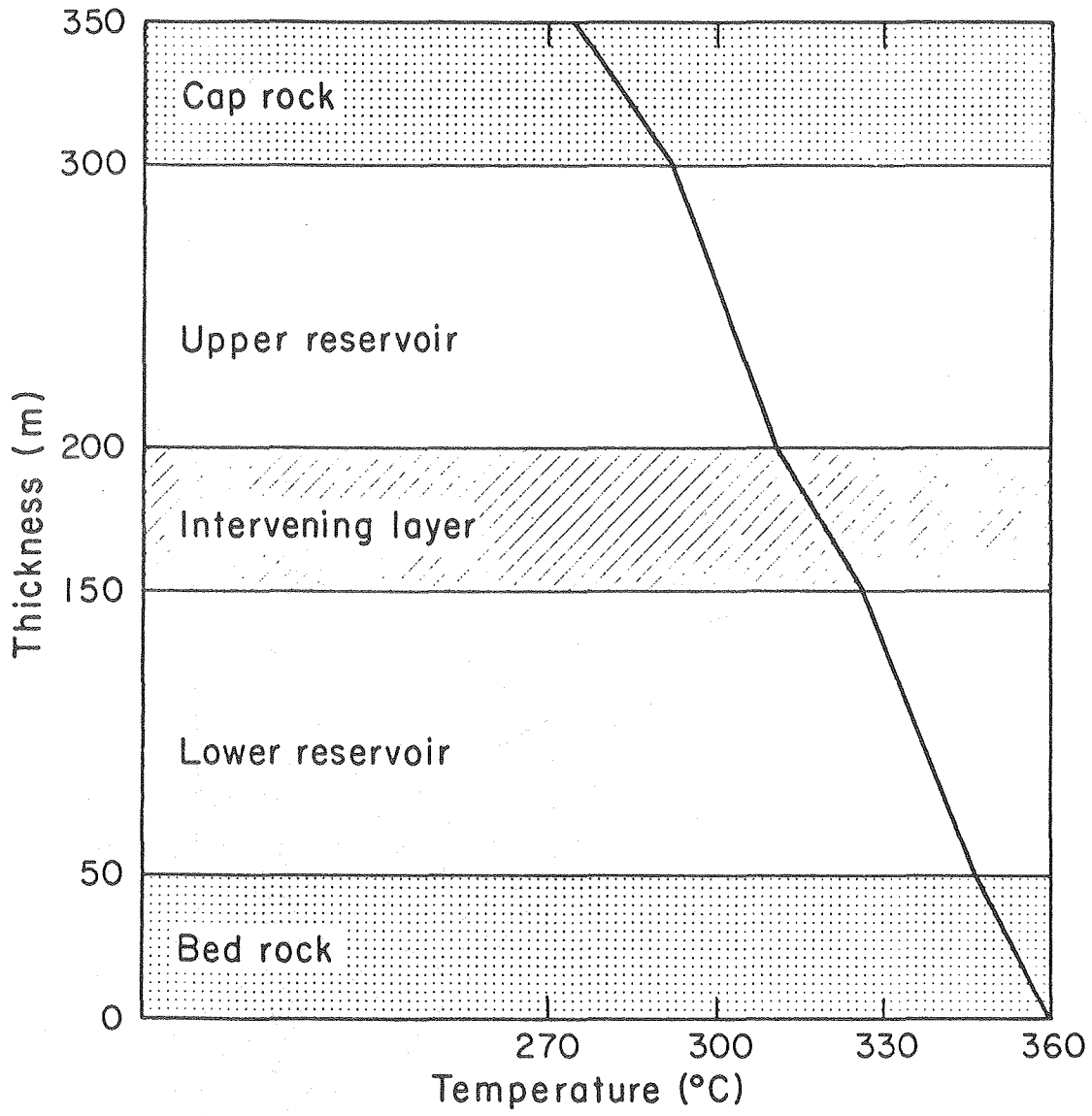
XBL 815-2982

Figure 28



XBL 815 - 2983

Figure 29



XBL 803-6829

Figure 30